Preprints (www.preprints.org) | NOT PEER-REVIEWED | Posted: 30 August 2021 doi:10.20944/preprints202108.0536.v1

Article

Alphavirus-driven interferon gamma (IFNg) expression inhibits tumour growth in orthotopic 4T1 breast cancer model

Olga Trofimova [1], Ksenija Korotkaja[1], Dace Skrastina[1], Juris Jansons[1], Karina Spunde[1], Maria Isaguliants[2,3,4] and Anna Zajakina[1]*

[1] Latvian Biomedical Research and Study Centre, Ratsupites Str.1. k.1., LV-1067 Riga, Latvia
[2] Riga Stradina University, Dzirciema iela 16, Kurzemes rajons, LV-1007 Riga, Latvia
[3] Department of Microbiology, Tumor and Cell Biology, Karolinska Institutet, 17177 Stockholm, Sweden
[4] N.F. Gamaleya National Research Center for Epidemiology and Microbiology, 123 098 Moscow, Russia
Authors' e-mails: OT: olj.trofimova@gmail.com, KK: ksenjakorotkaja@gmail.com; DS: dace.skrastina@biomed.lu.lv; JJ: jansons@biomed.lu.lv; KS: spunde.carina@gmail.com; MI: maria.issagouliantis@rsu.lv; AZ: anna.zajakina@gmail.com
* Correspondence: Correspondence: anna.zajakina@gmail.com

Abstract: Interferon gamma (IFNg) is a pleiotropic cytokine that can potentially reprogramme the tumour microenvironment. However, the antitumour immunomodulatory properties of IFNg still need to be validated due to variable therapeutic outcomes in preclinical and clinical studies. We developed a replication-deficient Semliki Forest virus vector expressing IFNg (SFV/IFNg) and evaluated its immunomodulatory antitumour potential *in vitro* in a model of 3D spheroids and *in vivo* in immunocompetent 4T1 mouse breast cancer model. We demonstrated that SFV-derived IFN-g stimulated bone marrow macrophages to acquire the tumoricidal M1 phenotype in 3D nonattached conditions. Coculturing SFV/IFNg-infected 4T1 spheroids with BMDMs inhibited spheroid growth. In the orthotopic 4T1 mouse model, intratumoural administration of SFV/IFNg virus particles alone or in combination with the Pam3CSK4 TLR2/1 ligand led to significant inhibition of tumour growth compared to the administration of the control SFV/Luc virus particles. Analysis of the composition of intra-tumoural lymphoid cells isolated from tumours after SFV/IFNg treatment revealed an increase in $CD4^+$ and $CD8^+$ and a decrease in T-reg ($CD4^+/CD25^+/FoxP3^+$) cell populations. Furthermore, a significant decrease in the populations of cells bearing myeloid cell markers CD11b, CD38 and CD206 was observed. In conclusion, the SFV/IFNg vector induces a therapeutic antitumour T-cell response and inhibits myeloid cell infiltration in treated tumours.

Keywords: interferon gamma; cancer immunotherapy; viral vectors; alphavirus; bone marrow-derived macrophages; spheroids; CD38; Pam3CSK4

1. Introduction

The tumour microenvironment (TME) and immune cell composition play essential roles in tumour development. Immunotherapy is a novel strategy for cancer treatment aimed at modifying the TME and (re)programming immune cells. Pleotropic cytokines represent key instruments of immunotherapy because they allow the programming of the TME for cancer treatment due to their ability to mediate communication between cells and modify their functions [1,2]. IFN-gamma (IFNg) has crucial impact on the organism immune response to tumours, including strong antiproliferative effects, modulation of adaptive and innate immune responses, activation of antigen-presenting cells by promoting the expression of MHC class I and II molecules on the cell surface, regulation of functions of T helper cells, activation of NK cells, and the ability to modify the functions of macrophages [3,4]. During the last 20 years, series of preclinical and clinical studies examined the therapeutic impact of IFNg alone or in combination with chemotherapy and immunotherapy. Despite all the efforts, there is still no definite conclusion on the efficacy of IFNg in cancer therapy [5-7]. One of the drawbacks is a systemic toxicity [6]. Furthermore,

© 2021 by the author(s). Distributed under a Creative Commons CC BY license.

Preprints (www.preprints.org) | NOT PEER-REVIEWED | Posted: 30 August 2021 doi:10.20944/preprints202108.0536.v1

the IFNg-related induction of proinflammatory responses was shown to lead to not only antitumour, but also protumour effects [8].

Vector-based intratumoural delivery of IFNg significantly increases therapeutic outcomes and reduces systemic toxicity. IFNg delivery by adenovirus [9,10], herpesvirus [11] and replication-deficient recombinant avian (fowlpox) virus vectors [12] showed promising results in animal models. Moreover, clinical trials testing antitumour effects of adenoviral vectors expressing IFNg reported positive outcomes in T and B cell lymphoma patients [13,14]. Intratumoural vector-based expression of IFNg not only reduced therapy toxicity but also restored the functions of immune cells in TME [15,16].

Recent reports indicate that tumor progression largely depend on the (activities of) tumour-associated myeloid lineage cells [17]. Myeloid-derived cells, as a multifunctional and highly heterogeneous cell population, have become a subject for extensive studies within the last five years, which has led to reconsideration or refining of the classic concepts of immune crosstalk in tumours and revised the role of IFNg and other cytokines in tumour development [8,18-20]. IFNg orchestrates leukocyte maturation and proinflammatory activation of myeloid cells. Classically, IFNg targets monocytes/macrophages and promotes their activation to the antitumoural M1 phenotype, whereas cancer cells promote myeloid cell infiltration and (re)program macrophages towards the tumour-supporting M2 phenotype [21]. However, several studies have indicated possible protumourigenic effects of IFNg through induction of genomic instability (e.g., copy number alterations) and/or an immunoevasive gene expression signature in cancer cells (PD-L1, PD-L2, CTLA-4, nonclassical MHC class Ib antigens, IDO1, etc.), which correlated with clinical observations [22]. A promising way to enhance the antitumour effects of IFNg along with the inhibition of its potential protumour effects is shown to be a complex treatment with immune checkpoint inhibitors [23-25], chemoimmunotherapy [26,27] alone or in combination with oncolytic viral vectors additionally inducing the innate immunity in tumours [28,29].

This study aimed to examine the anti-tumour effect of intratumoural expression of IFNg driven by alphaviral vector. Alphaviruses possess natural tumour tropism to mouse and human cancer cells, which has been documented in many preclinical studies [30, 31]. Recent studies indicate the synergistic antitumour activity of alphaviral vectors expressing cytokines when combined with checkpoint inhibitors (antibodies) and chemical drugs [32-34]. In contrast to other viruses, Semliki Forest virus (SFV) does not infect human and mouse macrophages [35], making the system suitable for functional SFV/IFNg-based programming of macrophages and initiation of downstream M1-related proinflammatory reactions in the TME.

In previous studies, IFNg showed synergistic proinflammatory macrophage activation with viral RNA, bacterial endotoxin lipopolysaccharide (LPS) and different specific Toll-like receptor (TLR) agonists [36-38]. Recently, we have demonstrated the ability of SFV-driven IFNg in combination with the TLR2/1 agonist Pam3CSK4 (a synthetic mimetic of bacterial lipopeptide - Pam3) to activate bone marrow-derived macrophages (BMDMs), which inhibited Lewis lung carcinoma cell growth in cocultured monolayers [35]. We suppose that SFV-driven expression of IFNg will enhance the antitumoural IFNg effects through induction of innate antiviral immunity in tumours in response to SFV replication. In the current study, we characterized the ability of the SFV/IFNg vector to activate BMDMs towards the M1 phenotype and evaluated its effect on 4T1 mouse breast cancer cells in a three-dimensional (3D) spheroid model *in vitro*. Furthermore, we applied SFV/IFNg alone or in combination with Pam3 for in vivo therapy of 4T1 tumour-bearing mice to evaluate tumour growth inhibition. We explored the immune cell composition of TME after SFV/IFNg treatment by flow cytometry, and discovered main changes occurring after treatment which we believe to be responsible for the observed antitumour effects.

Preprints (www.preprints.org) | NOT PEER-REVIEWED | Posted: 30 August 2021 doi:10.20944/preprints202108.0536.v1

2. Materials and Methods

Cell lines

For *in vitro* studies, 4T1-Fluc-Neo/eGFP-Puro cells (4T1/eGFP; Imanis Life Sciences, USA) were cultured in RPMI-1640 selection medium (Cat. No. 12-115F; Lonza™ BioWhittaker™, Walkersville, Maryland, USA) supplemented with 10% fetal bovine serum (FBS; Cat. No. FBS-HI-12A; Capricorn Scientific, Ebsdorfergrund, Hessen, Germany), 2 mM L-glutamine (Cat. No. 25030-024, Gibco, Thermo Fisher Scientific, Waltham, Massachusetts, USA), 1% penicillin/streptomycin (pe/st) (Cat. No. 15070-063, Gibco), 0.1 mg/ml G418 (Cat. No. 10131-027, Gibco, Life Technologies) and 2 μg/ml puromycin (Cat. No. ant-pr; InvivoGen, San Diego, CA, USA) or for 3D cultivation, in RPMI-1640 medium supplemented with 10% FBS, 2 mM L-glutamine, and 1% pe/st. BHK-21 cells were cultured in BHK-Glasgow MEM (Cat. No. 21710-025; Gibco, Life Technologies, UK) supplemented with 5% FBS, 10% tryptose phosphate broth (Cat. No. 18050-039; Gibco, Life Technologies), 2 mM L-glutamine, 20 mM HEPES (Cat. No. 15630-056, Gibco, Life Technologies), and 1% pe/st.

L929 cells (ATCC® CCL-1™, Manassas, Virginia, USA) producing murine macrophage colony-stimulating factor (M-CSF) were cultured to generate conditioned medium containing M-CSF. L929 cells were plated in RPMI-1640 with 10% FBS, 2 mM L-glutamine, and 1% pe/st in T175 flasks (Cat. No. 156502, Gibco) to achieve 60-70% confluence. Then, the medium was replaced with 30 ml of fresh medium, and the cells were incubated for 8-9 days in a humidified 5% CO_2 incubator at 37 °C. After cultivation, the conditioned medium (CM) from L929 cell culture was collected, centrifuged at 400 g for 10 min, transferred to a new tube and centrifuged again at 10,000 g for 20 min at 4 °C to remove cell pellets. The CM preparations of L929 cell medium were aliquoted and stored at -20 °C.

In vivo studies were made on murine mammary gland adenocarcinoma 4T1 cells (ATCC® CRL-2539™) and 4T1 cells expressing firefly luciferase 4T1(Luc2) (Bioware Ultra Cell Line 4T1luc2, Caliper Life Sciences Inc., Hopkinton, MA, USA). Adenocarcinoma 4T1 cells were cultured in DMEM-GlutaMAX (Cat. No. 31966-021, Gibco), 10% FBS, and 40 μg/ml gentamicin (Cat. No. 00-0442; Sopharma, Sofia, Bulgaria), and 4T1(Luc2) cells in RPMI-1640 supplemented with 10% FBS, 2 mM L-glutamine, and 1% pe/st. Cells were incubated in a humidified 5% CO_2 incubator at 37 °C and passaged using 0.05% trypsin solution (Cat. No. 15400-054, Gibco).

Formation of 4T1/eGFP spheroids

Three-dimensional (3D) scaffold-free 4T1/eGFP cell culture spheroids were generated in 96-well black round bottom ultralow attachment plates (Cat. No. CLS4515, Corning, Life Sciences, New York, USA) according to the manufacturer's instructions. Briefly, 4T1/eGFP cells were collected from monolayers by trypsin treatment, filtered through 40 μm cell strainers (Cat. No. CLS431750, Corning) and plated 3000 cells per well in a total volume of 100 μl of RPMI-1640 medium supplemented with 10% FBS, 2 mM L-glutamine, and 1% pe/st. The cells were incubated in a humidified 5% CO_2 incubator at 37 °C for 18-24 h, and then, the spheroids were used for infection with SFV vectors.

Expression vectors

The pSFV/Luc plasmid (a kind gift of A. Merits, University of Tartu, Estonia) has been previously described [39]. The pSFV1 and pSFV-Helper1 plasmids [40] were generously provided by H. Garoff (Karolinska Institute, Stockholm, Sweden). The pSFV/IFNg and SFV/DS-Red vectors were generated in our lab as described previously [35, 41].

Production of SFV virus particles

The plasmids pSFV/IFNg, pSFV/Luc, and pSFV-Helper1 were linearized with the restriction enzyme SpeI (Cat. No. ER1251; Thermo Fisher Scientific). One microgram of each linearized plasmid was used for in vitro SFV-Helper1 RNA and recombinant RNA (SFV/IFNg, SFV/Luc, SFV/DS-Red) synthesis using SP6 RNA polymerase (Cat. No. AM2071; Thermo Fisher Scientific) as described previously [41]. For packaging of RNAs

Preprints (www.preprints.org) | NOT PEER-REVIEWED | Posted: 30 August 2021 doi:10.20944/preprints202108.0536.v1

into viral particles, each recombinant RNA was co-electroporated (850 V, 25 µF, two pulses) with SFV-Helper1 RNA into 1×10^7 BHK-21 cells using a Gene Pulser-II apparatus (Bio-Rad, Hercules, CA, USA). The electroporated BHK-21 cells were cultured in T75 tissue culture flasks in 15 ml of BHK-Glasgow MEM supplemented with 5% FBS medium in a humidified 5% CO_2 incubator at 33 °C for 48 h. After cultivation, virus-containing supernatant was harvested from BHK-21 cells, clarified by centrifugation (Eppendorf fixed-angle rotor 5804, 10,000 g, 20 min, 4 °C), filtered through a vacuum 0.22 µm pore filter (Cat. No. 83.1822.001, Sarstedt, Newton, North Carolina, USA) and concentrated by ultracentrifugation through double sucrose cushions (50% and 20% sucrose in TNE buffer) as previously described [42]. Briefly, 30 ml of filtered virus-containing medium was carefully overlayed onto a sucrose step gradient and centrifuged using a SW 32 Ti rotor (Beckman Coulter, Brea, Ca, USA) at 150,000 g for 90 min at +4 °C. The virus-containing fractions (2 ml) were collected from the bottoms of the pierced tubes, and dialyzed using dialysis cassettes (Cat. No. 02906-36; Spectra/Por, USA) for 4-5 h against TNE buffer. Virus preparations were aliquoted, frozen in liquid nitrogen and stored at -80 °C. The viral titres (infectious units per ml, i.u./ml) were quantified by infecting BHK-21 cells seeded in 24-well plates. The day after infection, viral titres were quantified by immunostaining with anti-SFV nsp1 antibody (a kind gift from Prof. A. Merits, Tartu, Estonia) as previously described [39].

Isolation and culturing of bone marrow-derived macrophages (BMDMs)

Murine BMDMs were isolated from bone marrow progenitors obtained from BALB/c mice as previously described [43,44]. Briefly, mouse femurs and tibias were dissected from 8- to 10-week-old BALB/c mice, and bone marrow cells were collected by flushing the femurs and tibias with 2-5 ml of RPMI-1640 supplemented with 10% FBS, 2 mM L-glutamine and 1% pe/st (RPMI 10% FBS) using a 25 G needle. After the cells were centrifuged for 5 min at 400 g, the erythrocytes were lysed in 3 ml of lysis buffer (Cat. No. A10492-01; Gibco, Life Technologies) for 5 min at RT. The activity of lysis buffer was stopped with 10 ml of RPMI with 10% FBS and centrifuged at 400 g for 5 min. Next, the cells were resuspended in 10 ml of RPMI 10% FBS, and the cell suspension was filtered through a 70 µm cell strainer (Cat. No. 800070; BioSwisstec, Schaffhausen, Switzerland) and centrifuged at 400 g for 5 min. The cells were seeded onto 100 mm untreated cell culture dishes (Cat. No. 0030702018; Eppendorf, Hamburg, Germany) in complete BMDM cultivation medium (RPMI-1640 with 10% FBS and 30% L929-CM containing M-CSF, 2 mM L-glutamine, 1% pe/st) at a concentration of 8×10^5 cells/ml and cultured for 7 days at 37 °C and 5% CO_2. After 7 days of cultivation, cells that were not immediately used in the experiment were frozen and stored in liquid nitrogen.

Cryotubes containing BMDMs were removed from liquid nitrogen storage and immediately placed in a 37 °C water bath. After the cells were taken up from frozen stasis, they were immediately added to 12 ml of 37 °C prewarmed RPMI with 10% FBS solution, mixed by inverting several times, and centrifuged for 7 min at 400 g. After centrifugation, the cells were washed with 10 ml of RPMI with 10% FBS twice and seeded in 100-mm untreated cell culture dishes in BMDM complete growth media containing 30% L929 CM. Cells were cultivated for 6 days at 37 °C and 5% CO_2, and the medium was changed two times. On day 10, cells were detached from the plate with cold PBS, washed and resuspended in complete media containing 10% L929 CM. Then, cells were counted and seeded in a monolayer (2D) on-to 12-well plates (Cat. No. 0030721012; Eppendorf) at a concentration of 2×10^5 cells/ml per well, or into a 96-well black round bottom ultralow attachment plate in the amount of 10^5 cells per well in 200 µl, to provide 3D conditions for cell incubation at a concentration of 10^5 per well in 200 µl. Cells were incubated overnight at +37 °C and 5% CO_2 and then used for macrophage polarization experiments.

BMDM polarization towards the M1 phenotype with virus-derived IFNg (vdIFNg)

Preprints (www.preprints.org) | NOT PEER-REVIEWED | Posted: 30 August 2021 doi:10.20944/preprints202108.0536.v1

Cell culture supernatant containing vdIFNg was obtained by infection of BHK-21 cells with SFV/IFNg virus at a multiplicity of infection of 1 (MOI=1) as previously described [35]. The control supernatant of infected cells (vdLuc-control, not containing IFNg) was obtained by infection of BHK-21 cells with SFV/Luc virus under the same conditions (MOI=1). The vdIFNg in the supernatant was quantified by mouse IFNg ELISA (Cat. No. 88-7314-22; Invitrogen). The supernatants were aliquoted, frozen and used subsequently for 2D and 3D macrophage polarization experiments. According to the IFNg ELISA, the stock solution contained 2 µg/ml vdIFNg.

For M1 polarization, BMDM medium was supplemented with vdIFNg and Pam3 (Cat. No. tlrl-pms; InvivoGen) to achieve final concentrations of 50 ng/ml vdIFNg and 50-100 ng/ml Pam3, respectively. In the control experiments, the BMDMs were cultured under 2D or 3D conditions in BMDM complete medium supplemented with an equivalent amount (µl) of supernatant collected from the SFV/Luc-infected BHK-21 cells (vdLuc). Untreated BMDMs (M0) served as an additional control. Cells were incubated for 2 days at +37 °C 5% CO_2.

Analysis of BMDM polarization by flow cytometry

After two days of macrophage incubation with vdIFNg and vdLuc (control), the cells were harvested for further flow cytometry analysis. For collection of cells from 96-well ultralow attachment plates (3D culture), the content of each well was mixed by pipetting and transferred into an 1.5 ml Eppendorf tube. The cells from at least 4 wells were combined and centrifuged at 500 g for 10 min to obtain a sufficient number of cells for immunostaining and flow cytometry. For detachment from 12-well plates (2D culture), wells were treated with cold PBS at 4 °C for 20 min. Then, the content of the wells was flushed by pipetting, collected into an Eppendorf tube and centrifuged at 500 g for 10 min. Cells from at least two wells were combined.

For immunostaining, the cells (2D and 3D) were washed twice with PBS containing 10% FBS (PBS-FBS), resuspended in 100 µl of PBS-FBS containing 12.5 µg/mL mouse IgG (Cat. No. I8765-5MG, Sigma-Aldrich, Co., LLC, St. Louis, Missouri, USA) to block nonspecific antibody binding and incubated for 30 min at 4 °C. After blocking, the cells were washed with PBS-FBS and stained in 50 µl of PBS-FBS with fluorophore-labelled monoclonal antibodies: anti-CD11b-FITC (Cat. No. 11-0112-82; Invitrogen), anti-MHC II-PE (Cat. No. 12-5321-82; Invitrogen), anti-CD206-BV421 (Cat. No. 141717; Biolegend) and anti-CD38-PerCP-eFluor 710 (Cat. No. 46-0381-82; Invitrogen), diluted as recommended by the manufacturers. Cells were incubated with antibodies for 1 h at 4 °C, washed twice with PBS-FBS and intracellular staining was performed with anti-iNOs-APC-eFluor 780 (Cat. No. 47-5920-82) and anti-Arginase 1-APC antibodies (Cat. No 17-3697-82; both from Invitrogen). The PerFix-nc kit (Cat. No. B31168; Beckman Coulter) was used according to the manufacturer's instructions. Briefly, the cells were suspended in 25 µl of FBS, 15 µl of Fixative reagent was added, the mixture was vortexed and incubated for 15 min at room temperature. Then, 150 µl of permeabilizing reagent was added to each tube, and immediately after membrane permeabilization, the anti-iNOs and the anti-Arginase 1 antibodies were added in recommended amounts, and incubated for 30 min at room temperature in the dark. Finally, 1.8 ml of final reagent solution was added to the cells. Stained cells were kept at +4 °C and analysed the next day by FACSAria BD Hardware flow cytometer using FACSDiva Software (BD Biosciences, San Jose, CA, USA). The experiment was repeated twice, and each staining was performed in duplicate. The data were analysed by FlowJo 10.3 software (FlowJo LLC, Ashland, Oregon, USA) and presented as the mean of two independent experiments.

Nitric oxide assay

To determine the level of nitric oxide in activated BMDM cell culture medium, we used a nitric oxide assay kit (Cat. No. EMSNO; Invitrogen). The determination of the amount of nitric oxide was based on the detection of nitrite levels in cell culture media.

Preprints (www.preprints.org) | NOT PEER-REVIEWED | Posted: 30 August 2021 doi:10.20944/preprints202108.0536.v1

Briefly, 50 µl of cell culture media was collected from each well, clarified by centrifugation and used for NO quantification. The nitrite standards provided by the kit were used for standard curve generation and NO quantification. The optical density was measured at 540 nm using a spectrophotometer. The data are presented as the mean value of two independent experiments, and each sample in triplicate.

Infection of 4T1/eGFP spheroids with recombinant SFV viruses

The SFV/DS-Red, SFV/Luc and SFV/IFNg virus stock solutions were diluted in PBS (containing Mg^{2+} and Ca^{2+}, PBS-Ca/Mg) to achieve concentrations of 5×10^5 (SFV/Luc and SFV/IFNg) and 1×10^6 (SFV/DS-Red) viral particles (i.u.) per 1 ml. Spheroids were washed twice with PBS-Ca/Mg: 200 µl of PBS-Ca/Mg were added to each well to the spheroids grown in 100 µl of the cultivation medium and carefully removed immediately after avoiding the loss of the free-floating spheroids. Next, 100 µl of the solution containing virus particles was added to each well to achieve 5×10^4 (SFV/Luc and SFV/IFNg) or 1×10^5 (SFV/DS-Red) i.u./well. The control cells were incubated with PBS-Ca/Mg. The spheroids were incubated at 37 °C for 1 h and 10 min on a shaker at 40 rpm (3D Sunflower mini-shaker, BS-010151-AAG, Bio-San, Riga, Latvia), additionally, infection without shaking was tested. After incubation, 100 µl of virus-containing solution was removed from each well, and 150 µl of RPMI with 10% FBS was added. Immediately after, 150 µl of cell media was removed from each well and replaced with fresh 100 µl of RPMI supplemented with 10% FBS. Infected spheroids were incubated in a humidified 5% CO_2 incubator at 37 °C.

Spheroid confocal microscopy

For confocal fluorescence microscopy, 4T1/eGFP spheroids were infected with SFV/DS-Red virus as described above, cultured for 2 days at 37 °C and 5% CO_2, and subjected to confocal laser scanning microscopy using a Leica TCS SP8 Laser DPSS561 with the following confocal settings: pinhole 70.7 µm and scan speed 400 Hz. The fluorescence was detected as follows: eGFP excitation laser 488 nm and emission detector PMT 2 (493-560 nm); Ds-Red excitation laser 561 nm and emission detector HyD (573-651 nm). The fluorescence intensity profiles from the spheroid upper rim to the bottom were acquired using a z-stack of 48 focal planes with a step pass of 5 µm. The images were analysed by LasX 3.1.5 software. Total fluorescence intensity (eGFP and DS-Red profiles) was calculated for each spheroid, and at least four spheroids were analysed in each group. Through imaging, all the measurement conditions were kept constant for all experiments. The experiment was repeated twice.

Fluorimetry of 4T1/eGFP spheroids infected with SFV vectors and cocultured with BMDMs

The 4T1/eGFP spheroids (3000 cells/well) were infected with SFV/IFNg or SFV/Luc viruses at a virus dose of 5×10^4 i.u./well without plate shaking as described above. The next day after infection, the spheroid supernatants (50 µl) were collected to measure the IFNg production by ELISA (Cat. No. 88-7314-22; Invitrogen). Then, the BMDMs were added to the spheroids at a concentration of 3×10^4 cells in 100 µl of BM medium (10% L929 CM) per well (day 0). Pam3 ligand was added to wells to a final concentration of 50 ng/ml. The dynamics of spheroid growth were measured by an eGFP fluorimetry assay using Victor3V 1420-040 Multilabel HTS Counter (PerkinElmer, Waltham, Massachusetts, USA) with an emission filter of 485 nm and a detection filter of 535 nm. To prevent liquid evaporation from wells, we added 40-50 µl of fresh spheroid medium to each well every second day after fluorimetry. The total fluorescence was measured every second day, from individual measurements (each group, n=6-8); the data were presented as the mean fluorescence (a.u.) ±standard deviation. The experiment was repeated twice. Additionally, for microscopy visualization, detached macrophages were labelled with fluorescence dye (CellTracker CM-DiI, Cat. No. C7001, Thermo Fisher, or a similar dye providing unspecific labelling of cells), washed with cell medium, added to the infected spheroids as described above and cultivated for at least 7 days until macrophage labelling was detectable.

Preprints (www.preprints.org) | NOT PEER-REVIEWED | Posted: 30 August 2021 doi:10.20944/preprints202108.0536.v1

For visual control of spheroid growth, fluorescence microscopy of the spheroids was performed with labelled/unlabelled macrophages using inverted contrasting microscope Leica DM-IL (Leica Microsystems, Wetzlar, Germany). All experiments with labelled macrophages were repeated at least three times.

Experiments with animals and in vivo imaging

Female BALB/c mice (6-7 weeks of age) were purchased from the Laboratory Animal Centre, University of Tartu (Tartu, Estonia). The mice were housed 5 per cage in a climate-controlled room (temperature 22±2 °C and humidity 50±10%) under a 12 h light/dark cycle and provided a standard diet and water ad libitum. All animal experimental protocols were approved by the Latvian Animal Protection Ethical Committee of Food and Veterinary Service (Permit Nr. 93, from December 11., 2017, Riga, Latvia).

Coinjection of 4T1(Luc2) cells with BMDMs

Treatment of 4T1 tumours with M1 macrophages polarized by vdIFNg was tested in the orthotopic (orth.) murine model. For this, before the implantation, aliquots of 1×10^4 cells 4T1(Luc2) cells were mixed with either 2×10^4 M0 (4T1(Luc2)+M0) or 2×10^4 M1-like cells activated with vdIFNg/Pam3 (4T1(Luc2)+M1) in total volume of 50 µl. BALB/c mice (n=5 per group) were injected with 50 ul of either 4T1(Luc2)+M0 or 4T1(Luc2)+M1 cell suspensions into the right thoracic mammary gland fat pads (day 0).

For bioluminescence imaging, mice received an intraperitoneal injection of 200 µl of D-luciferin potassium salt solution (XenoLight D-Luciferin, PerkinElmer) in PBS at a dose of 0.15 mg of D-luciferin per 1 g weight of each animal. Ten minutes after the injection of D-luciferin, the mice were anaesthetized with isoflurane/oxygen and placed in an in vivo imaging system (IVIS Spectrum, Perkin Elmer) as described by us previously [45]. The bioluminescence from injection sites was assessed every second day. After 15 days, the mice were anaesthetized and humanely sacrificed, the tumours were dissected and weighed. The lungs were removed and placed in 24-well plates to monitor infiltration of tumor cells (IVIS, Perkin Elmer) as previously described [46]. The data were analysed using the total photon flux emission (photons/second) in the regions of interest (ROI) using Living Image®, version 4.5 (PerkinElmer).

Treatment of 4T1 tumours with SFV vectors

Treatment of 4T1 tumours with SFV vectors was tested in both orthotopic and subcutaneous (s.c.) 4T1 models of breast cancer. In the orth. model, 4T1 cells were similarly suspended in PBS, and 50 µl of cell suspension containing 1.25×10^5 cells/50 µl was injected into the right thoracic mammary gland fat pads (day 0). In the sc. model, 4T1 cells were suspended in PBS, and 100 µl of cell suspension containing 2.50×10^5 cells/100 µl was subcutaneously injected above the right shoulder blade of each mouse (day 0). When the tumours became palpable - day 7 for s.c. tumours and day 4 for orth. tumours - an intratumoural (i.t.) injection (100 µl) of SFV vectors (or PBS as a control) was performed: 4×10^7 i.u. of SFV/IFNg or SFV/Luc per tumour, respectively. The repeated vector i.t. injections were performed at day 13 (s.c. tumours) and at day 10 (orth. tumours) with the same virus dose. The next day after virus treatment mice were intra-tumourally injected with Pam3 ligand (Pam3CSK4) dissolved in PBS in the amount of 10 µg/60 µl and 15 µg/90 µl per each tumour. The tumour diameters were measured using digital electronic callipers, and the tumour volume in mm^3 was calculated using the following formula: $V=(width^2\times length)/2$. At day 17 (s.c. tumours) and at day 14 (orth. tumours), the animals were anaesthetized and sacrificed, and the tumours were removed, weighed and subjected to immune cell isolation for flow cytometry. The tumour inhibition rate (IR, %) was calculated as follows: IR=100–(mean weight of treated tumours/(mean weight of PBS control tumours × 100%).

Flow cytometry analysis of intratumoural immune cells

Preprints (www.preprints.org) | NOT PEER-REVIEWED | Posted: 30 August 2021 doi:10.20944/preprints202108.0536.v1

Tumours were homogenized with 3-4 ml of collagenase A (Cat. No. 10103586001; Roche, Basel, Switzerland) at 1.5 mg/ml and DNase at 15 µg/ml (Cat. No. ENZ-417; ProSpec Medical Holding, Los Angeles, CA, USA) in DMEM and incubated for 1 h on a magnet stirrer at 37 °C. After the enzymatic reaction was stopped with 8-10 ml of ice-cold DMEM with 10% FBS, the cells were filtered through a 70 µm strainer and centrifuged at 400 g for 10 min. Then, the cells were resuspended in 3 ml of erythrocyte lysis buffer (Cat. No. A10492-01; Gibco, Life Technologies), and incubated for 5 min at RT. The activity of lysis buffer was stopped with 10 ml of RPMI with 10% FBS. Next, the cells were centrifuged at 400 g for 5 min, and washed with 7-8 ml PBS-FBS two times. Then, the cells were counted with Countess Automated Cell Counter (Thermo Fisher Scientific Invitrogen), and 1×10^6 cells per staining was used for further procedures. The cells were resuspended in 100 µl of blocking solution containing 12.5 µg/ml mouse IgG diluted in PBS-FBS, and incubated for 30 min on ice. After blocking, the cells were washed with PBS-FBS and stained with fluorochrome-labelled monoclonal antibodies diluted as recommended by the manufacturers in 50 µl of PBS-FBS per staining. The following monoclonal antibodies were used: for mix 1 - anti-CD11b-FITC, anti-MHC II-PE, anti-CD206-BV421, and anti-CD38-PerCP-eFluor 710; for mix 2 - anti-CD3-FITC (Cat. No. 11-0032-82), anti-CD4-APC-eFluor 780 (Cat. No. 47-0041-82), anti-CD8-APC (Cat. No. 17-0081-82) and anti- CD25-PE (Cat. No. 12-0251-82) (all from Invitrogen) and incubated for 1 h at +4 °C. After staining, the cells were washed two times with PBS-FBS.

For intracellular staining with anti-iNOs-APC-eFluor 780 , anti-Arginase1-APC and anti-FoxP3-PerCP-Cyanine5.5 (Cat. No. 45-5773-82; Invitrogen) antibodies, the PercFix-nc kit was used according to the provided instructions. Briefly, the cells were suspended in 25 µl of FBS, and 15 µl of Fixative reagent was added, vortexed and incubated for 15 min at room temperature. Then, 150 µl of permeabilizing reagent was added to each tube. Immediately after membrane permeabilization, anti-iNOs and anti-Arginase 1 were added to mix 1, and anti-FoxP3 was added to mix 2 at an appropriate dilution and incubated for 30 min at room temperature in the dark. Finally, 1.8 ml of final reagent solution was added to the cell suspension. Stained/fixed cells were stored at +4 °C and analysed within two days by FACSAria BD Hardware and BD FACSDiva Software. UltraComp eBeads™ (Cat. No. 01-2222; Invitrogen, Thermo Fisher Scientific) were used for the compensation matrix. Importantly, the tumour homogenization, cell isolation and respective staining with antibodies was done simultaneously within one day for all compared groups.

Flow cytometry data analysis

Data were analysed with FlowJo software version 10.3 (FlowJo, Ashland, Oregon, USA). The total population was determined based on SSC-A and FSC-A. Single cells were determined by FSC-A and FSC – H to exclude cell aggregates. The gate of each antibody was determined using an unstained control, after which the percentage of the expression level of each marker was defined.

Statistical analysis

The statistical analysis was performed with GraphPad Prism 7 software. Confocal images were statistically compared by two-way ANOVA and Tukey's multiple comparisons test. *In vitro* fluorimetry data were analysed by t-tests and two-way ANOVA. *In vivo* tumour growth and flow cytometric data were analysed by the Mann-Whitney nonparametric t-test; bioluminescence signals were analysed using repeated-measures two-way ANOVA Sidak's multiple comparisons test. *P* values of 0,05 or less were considered statistically significant.

Preprints (www.preprints.org) | NOT PEER-REVIEWED | Posted: 30 August 2021 doi:10.20944/preprints202108.0536.v1

3. Results

Generation of cancer cell spheroids and their infection with SFV vector (SFV/DS-Red)

Three-dimensional spheroids made from cancer cells are a relevant system to investigate the interactions between cancer cells, macrophages and the SFV/IFNg vector in this study. The general plan of the in vitro research was to establish a 3D model to evaluate whether the SFV/IFNg vector, through infection of 4T1 mouse breast cancer cells, can induce a tumour suppressive phenotype in macrophages (M1), followed by the assessment of the therapeutic potential of the SFV/IFNg vector *in vivo*.

First, we evaluated the ability of the SFV vector to deliver transgenes to spheroids under 3D infection conditions. For this purpose, we generated eGFP-producing 4T1 spheroids (4T1/eGFP) cultured for 18 hours in nonadherent 96-well plates at a concentration of 3×10^3 cells in 100 µl. The cancer cells, in contrast to macrophages, aggregated and formed a tight 120-150 µm in diameter single spheroids within 18 h of incubation of the cell suspension in each well. The 4T1/eGFP spheroids were infected with SFV/DS-Red virus (1×10^5 i.u. per well), and DS-Red gene expression was analysed by live fluorescence confocal microscopy at 48 h post-infection (Fig. 1a, maximum intensity projection images). The confocal z slices of each spheroid were acquired every 5 µm for a total of 48 imaging planes, and the mean fluorescence intensity of every confocal slice was plotted as a function of its z depth (Fig. 1b). The image analysis revealed that the DS-Red-positive cells were mostly located on the surface of the spheroids with nonhomogeneous penetration into the spheroid (Fig. 1b). As expected, shaking of the spheroid plate during incubation with a virus significantly enhanced the infection efficiency (total DS-Red fluorescence intensity) and penetration of the virus into deeper spheroid slices (Fig. 1c, b). We concluded that the SFV vector infects the 4T1 spheroids in 3D conditions; however, virus spread within the spheroid is limited. Furthermore, confocal microscopy images revealed different growth patterns of infected and uninfected spheroids. Infected spheroids displayed less total eGFP fluorescence signal, $p<0,0001$ (Fig. 2c), and the size of the spheroids was visually smaller, indicating the inhibitory effect of the infection.

SFV-derived IFNg activates BMDMs towards an M1-like phenotype in 3D conditions

Next, we examined the ability of SFV virus-derived IFNg (vdIFNg, a supernatant from the cells infected with SFV/IFNg) to polarize macrophages to an M1-like tumour suppressive phenotype and the ability of these M1 macrophages to inhibit 4T1 spheroid growth in a 3D model. Recombinant IFNg in the presence of TLR ligands (such as LPS, Pam3) was shown to polarize BMDMs to the M1 phenotype when the cells are seeded on a standard 2D attachment plate [38]. Here, for the first time, we evaluated M1 polarization under free-floating conditions (3D) compared to standard 2D cell cultivation using vdIFNg and Pam3 TLR ligands.

BMDMs were seeded either in 12-well attachment plates to achieve a monolayer (2D) or into 96-well ultralow attachment plates at a relatively high cell density (10^5 cells per 96-well). The next day, the cell medium was supplemented with vdIFNg and Pam3 to trigger M1 polarization. Cell culture supernatant from SFV infected cells may contain multiple mediators of the innate cell immune response (e.g., type I IFNs) which can potentially affect macrophage polarization. To account for their effect, we used control supernatants of BHK-21 cells infected with SFV/Luc virus (vdLuc; see methods). BMDMs treated with vdLuc supernatant were considered as M0 undifferentiated cells ("M0 control"). Practically, we did not detect any differences between vdLuc control and untreated M0 (PBS) macrophages in this study. Nevertheless, these controls were used in all experiments.

Polarized macrophages were subjected to nitric oxide assays and flow cytometry analysis. The ability to produce nitric oxide (NO) is one of the main characteristics of pro-inflammatory M1-like macrophages. To assess NO levels in cell culture media, nitrites, as the product of nitric oxide oxidation, were quantified by the Griess test. Nitric oxide assays showed that treatment of BMDMs with vdIFNg and Pam3 in 2D and 3D conditions induced strong NO production (Fig. 2a). The maximal NO production, dependent on the

Preprints (www.preprints.org) | NOT PEER-REVIEWED | Posted: 30 August 2021 doi:10.20944/preprints202108.0536.v1

number of seeded cells, was observed on days 2-3 of cultivation. Treatment with vdLuc supernatant (M0 control) did not enhance the production of nitric oxide by macrophages (Fig. 2a).

Expression of macrophage polarization markers was analyzed by flow cytometry. The panmacrophage CD11b surface marker was detected in 80-90% of BMDMs and was decreased upon cultivation in 3D conditions ($p<0,05$; Fig. 2b). BMDMs activated by vdIFNg revealed a significant increase in the M1-like phenotype-specific markers MHCII, CD38 and intracellular inducible NO synthase (iNOs) (Fig. 2b, c). While MHCII expression did not show significant differences under 2D and 3D conditions, the levels of the CD38 and iNOs M1 markers were higher in 3D than in 2D conditions (CD38, $p=0,0180$ and iNOs, $p=0,0028$; Fig. 2b).

As expected, the level of CD206 (a classic marker of M2 macrophages [47] did not show significant changes depending on cell activation status and was relatively low in all groups (<2%). Interestingly, the level of Arginase 1, which is considered a predominant marker of M2-like macrophages [48], was increased in both vdIFNg groups (2D and 3D, Fig. 2b). Several studies have shown that overexpression of Arginase 1 in the M1 population could be due to the presence of the TLR2/1 ligand Pam3 [49].

In summary, we concluded that macrophages can be effectively activated to an M1-like phenotype under 3D free-floating conditions using vdIFNg/Pam3 treatment, which, in general, resembles the 2D characteristics of M1 macrophages.

SFV/IFNg infection of the 4T1/eGFP spheroids inhibits spheroid growth in the presence and absence of macrophages

The 4T1/eGFP spheroids were infected with equal amounts of either SFV/IFNg or SFV/Luc viruses or incubated with PBS. We used relatively low virus dose for infection (5×10^4 i.u./spheroid) to avoid significant inhibition of spheroid growth by virus infection itself, which may mask the inhibitory effect of macrophages. Moreover, spheroid infection with such an SFV/IFNg virus dose provided up-to 15 ng/ml of vdIFNg production, as confirmed by quantitative anti-IFNg ELISA (Fig. 3a), which is sufficient amount for macrophage activation [35, 38]. The day after spheroid infection with SFV, BMDMs (M0) were added (day 0). To confirm macrophage activation to the M1 pro-inflammatory phenotype, we assessed the presence of NO in cell media after two days of macrophage incubation with infected spheroids and the uninfected control (day 2), which showed NO production levels similar to those in 2D and 3D conditions without spheroids (Fig. 3a, Fig. 2a).

Spheroid growth was measured by fluorimetry every second day for 10 days to assess the inhibitory effect of macrophages in the presence or absence of SFV vectors (Fig. 3b). For this, twelve groups of combinations of spheroids (sph) with/without macrophages (M0), SFV vectors and/or Pam3 ligand were generated and the respective fluorimetry data were collected in total six fluorimetry measurements starting from day 0 (Supplementary Fig.S1a). Analysis of fluorimetry data at day 10 showed that the strongest inhibitory effect on the cancer cell spheroid growth was observed in the sph+SFV/IFNg+Pam3+M0 and sph+SFV/IFNg+Pam3 groups (Fig. 3b). Interestingly, macrophages and SFV/IFNg independently inhibited spheroid growth in all groups compared to the untreated or SFV/Luc treated groups (sph and sph+M0 ($p<0,0001$); sph+Pam3 and sph+Pam3+M0 ($p<0,0001$); sph+SFV/Luc and sph+SFV/IFNg ($p<0,0001$); sph+SFV/Luc+Pam3 and sph+SFV/IFNg+Pam3 ($p<0,0001$); Fig. 3b)

Very high ($p<0,0001$) differences were revealed between untreated and treated spheroids: sph and sph+SFV/IFNg+Pam3+M0; sph and sph+SFV/IFNg+Pam3 (Fig. 3b). Although both SFV/IFNg and M0 showed inhibitory effects on the spheroid growth, on day 10 the inhibitory effect of sph+SFV/IFNg+Pam3+M0 combination was significantly higher than of the combination without macrophages sph+SFV/IFNg+Pam3, $p<0,001$, pointing at the inhibitory role of macrophages in tested system. Measurement of NO in all groups at day 4 demonstrated that combination sph+SFV/IFNg+Pam3+M0 triggered potent production of NO (40 μM; Supplementary Fig.S1b). Furthermore, these data (Fig. 3b,

Preprints (www.preprints.org) | NOT PEER-REVIEWED | Posted: 30 August 2021 doi:10.20944/preprints202108.0536.v1

Supplementary Fig.S1b) was supported by the quantification of luminescence signal produced by the spheroid lysates prepared at day 10 (Supplementary Fig.S1c). Altogether, this demonstrated the inhibition of spheroid growth in the presence of SFV/IFNg and macrophages compared to the untreated controls ($p<0,0001$).

We concluded that SFV infection in combination with macrophages provided the most significant inhibition of spheroid growth (Fig. 3b). The inhibitory effect of SFV/IFNg could be explained by the known cytostatic effect of IFNg, the inhibitory effects of M0 on their own is unclear. To dissect the effects, we visualized 4T1/eGFP spheroid growth in the presence of fluorescently labelled macrophages (Fig. 3c). The infection of spheroids with SFV/IFNg prevented the migration/distribution of 4T1/eGFP cells within the well. On contrary, M0 macrophages stimulated migration of 4T1/eGFP cells out of the spheroids (Fig. 3c, day 7; Supplementary Fig.S2, day 6 and day 10). This migration would eventually lead to the diminishment of fluorescence signal from the spheroids, interpretable as inhibition of spheroid growth. The effect of Pam3 on spheroid growth remains to be investigated in a separate study.

Inhibition of growth of 4T1luc2 tumour cells by M1 macrophages in BALB/c mice

Both, macrophages M0 and SFV/IFNg vector, have demonstrated inhibitory effects on the spheroid growth, so it was unclear whether vdIFNg-activated M1 macrophages can preferentially suppress tumour growth compared to M0 macrophages. We sought to prove this in *in vivo* settings by evaluating the effect of M1-like macrophages pre-polarized by vdIFNg treatment on the growth of 4T1 tumors in BALB/c mice.

We used an *in vivo* imaging system (IVIS) to measure tumour growth in mice in the presence of M0- or vdIFNg-polarized M1 macrophages, which were coinjected orthotopically together with 4T1(Luc2) cells (day 0). Tumour growth was monitored by in vivo bioluminescence imaging (BLI) assessing the photon flux emitted by 4T1(Luc2) cells every second day (Fig. 4). Coinjection of 4T1luc2 cells with M1 macrophages significantly delayed tumor growth, as could be seen from the comparison of bioluminescent signals released from the sites of implantation of 4T1(Luc2)+M1 compared to 4T1(Luc2)+M0 cells (days 7 and 9 post implantation; $p<0.05$; Fig. 4a,b). No difference in bioluminescence from 4T1(Luc2)+M1 compared to 4T1(Luc2)+M0 derived tumors was observed at the later time points when bioluminescence signal was close to saturation ($p>0.1$; Fig. 4a,b). However, on day 15 when mice were sacrificed, tumour weight in the M1 co-injected group was found to be significantly lower than in M0 group ($p=0,0278$; Fig. 4c).

We have also assessed infiltration of tumor cells into the distal organs, namely lungs as the organ mostly affected in 4T1/4T1luc2 model [45]. For this, we assessed the bioluminescent signal emitted by organs by ex vivo imaging performed immediately after their dissection as previously described [46]. Bioluminescent signal emitted by lungs of 4T1(Luc2)+M1 and 4T1(Luc2)+M0 implanted mice did not differ (Fig. 4b, c), indicating that M1 macrophages had no long-term effect on the migration of tumor cells registered by the experimental end-point.

To characterize the populations of the intra-tumoural immune cells, we homogenized tumours and subjected cell suspensions to the analysis by flow cytometry to identify the percentage of myeloid and lymphoid cells (Fig. 5). Myeloid cells were characterized by the pan-myeloid marker anti-CD11b. We revealed a significant decrease in the $CD11b^+$ cell population in 4T1luc2+M1 compared to 4T1luc2+M0 tumours ($p=0.0278$; Fig. 5a). Most of the $CD11b^+$ cells were found to express MHCII (up-to 80%, Supplementary Fig. S3). M1 and M0 tumours did not differ in % of $MHCII^{high}$ cells, neither within $CD11b^+$population, nor within total tumour cell population ($p>0.1$; Fig. S3). This was in contrast to the results of *in vitro* BMDM analysis, where MHCII receptor was highly expressed only by M1-polarized $CD11b^+$ cells (Fig. 2c). Interestingly, although M1 co-injected tumours demonstrated a decrease in the population of $CD11b^+$ cells, the presence of $CD11b^+/CD38^+$ cells in M1 tumours was significantly higher than that in the M0 group ($p=0.0078$; Fig. 5b).

Preprints (www.preprints.org) | NOT PEER-REVIEWED | Posted: 30 August 2021 doi:10.20944/preprints202108.0536.v1

Cancer cells and tumour-associated fibroblasts reprogramme macrophages to the tumour-promoting M2 phenotype [48]. Surprisingly, although $CD206^+/CD11b^+$ double positive cells did not show the statistically significant changes in total tumour cells of M0 or M1 coinjected tumours(Fig. 5b), we observed the increase of $CD206^+$ cells in $CD11b^+$ population in M1 coinjected tumours, p=0,0159 (Supplementary Fig. S3). Furthermore, both arginase 1 ($Arg\ 1^+$) and inducible NO synthase ($iNOs^+$) intracellular markers increased in $CD11b^+$ population of cells isolated from M1 coinjected tumours, p=0,004; p=0,0159, respectively, whereas in total cells only $iNOs^+/CD11b^+$ double positive cell population was increased, p=0,0317, indicating on the pro-inflammatory profile of the myeloid cells (Supplementary Fig. S3).

The most important changes were revealed in the lymphoid cell population, specifically T-regulatory cells (T-regs). Although 4T1luc2+M1 and 4T1luc2+M0 tumours did not differ in populations of $CD4^+$ and $CD8^+$ T cells (Fig. 5a), 4T1luc2+M1 tumours had significantly lower numbers $CD25^+/FoxP3^+/CD4^+$ cells, indicating that M1 pre-treatment diminishes the population of intra-tumoural T-regs (compared to treatment with M0, p=0.0079; Fig. 5a).

Thus, comparison of the M0 and M1 co-injected tumours clearly demonstrated that treatment with M1 inhibits tumour growth and changes composition of the myeloid and lymphoid intratumoural cell subsets by inhibiting infiltration of CD11b+ cells, increasing proinflammatory $iNOs^+$ phenotype of the myeloid cells, and decreasing the number of T-regs in the TME.

Intratumoural injection of SFV/IFNg virus inhibits orthotopic 4T1 tumour growth

To evaluate the antitumoural potential of SFV/IFNg virus, we used orthotopic (orth.) and subcutaneous (sc.) 4T1 murine models (n=5). Two intratumoural (i.t.) injections of the vector (4×10^7 i.u./tumour) were performed: the first injection was given as soon as the tumours became palpable (day 7 for s.c. model; day 4 for orth. model); the second repeated injection was performed six days later (Fig. 6a, b; red arrows indicate the vector/PBS injections). Furthermore, to stimulate macrophage polarization to M1, we treated the mice with Pam3 ligand. The day after virus vector administration, the mice received i.t. injection of Pam3 ligand solution: 10 μg (first injection) and 15 μg (repeated injection) per tumour). Tumour growth was measured regularly during 17 (s.c.) and 14 (orth.) days. At the end of the experiments, the tumours were resected and weighed. The tumour growth curves for all individual animals are presented in supplementary figure S4 (Fig. S4). Although in the s.c. model, a trend of tumour growth inhibition was observed in the SFV/IFNg+Pam3-treated group, the tumour growth parameters and the final tumour weight varied within each group; therefore, the observed inhibition did not reach the level of significance (Fig. 6a). A statistical significance (Mann-Whitney t-test) of the tumour volume of groups treated with SFV/Luc (sc.SFV/Luc+Pam3) and SFV/IFNg (s.c.SFV/IFNg+Pam3) at the last day 17 reached the probability level p=0,2103 (nonsignificant).

In contrast to sc. tumours, the orthotopic model showed relatively homogeneous tumour growth parameters, demonstrating significant inhibition of tumour growth in the treated mice (Fig. 6b). Compared to the PBS group the inhibition of tumour growth in the mice treated with SFV/IFNg+Pam3 was stronger than that in the SFV/Luc+Pam3 group: PBS vs SFV/IFNg+Pam3 the last day tumour volume p=0,004 and the tumour weight p=0,004; PBS vs SFV/Luc+Pam3 the last day 14 tumour volume p=0,0476 and the tumour weight p=0,0159. There was also a significant difference between the SFV/IFNg+Pam3 and SFV/Luc+Pam3 groups (the last day tumour volume p=0,004 and the tumour weight p=0,004). The tumour inhibition rate of the SFV/IFNg+Pam3 treatment group versus the PBS group was 59,6 %, whereas SFV/Luc+Pam3 treatment reached only 27.8 % versus the PBS group, indicating the therapeutic activity of IFNg.

To exclude the potential inhibitory effect of Pam3 on its own activity, we tested Pam3 administration without viral vectors (Fig. 6c). Some studies have revealed the

Preprints (www.preprints.org) | NOT PEER-REVIEWED | Posted: 30 August 2021 doi:10.20944/preprints202108.0536.v1

antitumoural effect of Pam3 and other TLR agonists [50,51], but we did not observe any significant inhibition of 4T1 orthotopic tumour growth in the Pam3-treated mice in dose comparable or higher than used in previous studies.

Since the SFV/Luc vector in combination with Pam3 showed a remarkable tumour inhibitory effect, we also evaluated the antitumour potential of SFV vectors on their own without Pam3 administration. Our data demonstrate a significant inhibitory effect of SFV/IFNg without Pam3 compared to that of the PBS group (the last day tumour volume p=0,004 and the tumour weight p=0.0079) and to the SFV/Luc group (the last day tumour volume p=0,0159 and the tumour weight p=0.0476) (Fig. 6d). There were no differences between the PBS- and SFV/Luc-treated groups in the absence of Pam3 (the last day tumour volume p=0,3452 and the tumour weight p=0,5)

Remarkably, the tumour inhibition rate of the SFV/IFNg+Pam3 treatment group was higher than that of the SFV/IFNg alone group, 59.6% and 49,1%, respectively, versus the corresponding PBS groups. SFV/Luc+Pam3 exhibited antitumour activity with a tumour inhibition rate of 27.8%, whereas no inhibitory effect could be seen for Pam3 or SFV/Luc alone. Remarkably, the treatment of tumours with SFV/IFNg alone (inhibitory rate 49,1%) is more efficiently than the treatment with SFV/Luc+Pam3 (inhibitory rate 27.8%). Thus, the treatment with Pam3 promoted a weak anti-tumor effect of the control SFV/Luc virus, and strengthened the effect of IFNg expressing SFV/IFNg vector, while Pam3 on its own had no anti-tumor effect. Altogether, this indicate the efficacy of anti-tumor treatment mediated by IFNg.

Analysis of immune cell composition of the tumours treated with SFV/IFNg

Next, we proceeded to characterization of the therapeutic potential of IFNg delivered by replication deficient SFV vector. For this purpose, the tumours raised in mice receiving SFV/IFNg, or SFV/Luc, or PBS, but no Pam3 (Fig. 6d) were subjected to flow cytometry analysis to dissect the composition of tumour infiltrating immune cells. For this, the tumours were homogenized and stained with lymphoid and myeloid cell markers. We started the analysis with a forward scatter (FSC) and side scatter (SSC) gate to perform a preliminary identification of distinct cell populations [52]. As shown by the light scattering analysis, four common populations distributed according to the cell size and granularity were identified (Fig. 7a). Tumors predominantly contain the following distinct cell populations: P1 – cancer cells, endothelial cells, fibroblasts, different types of myeloid cells; P2 population – small agranular cells, typically related to T lymphocytes; P3 – monocytes; P4 – granulocytes. We found that the P2 population was significantly (p<0,01) increased in the SFV-treated tumours compared to the PBS-treated tumours (Fig. 7b, c).

Analysis of lymphocytes ($CD3^+$) revealed a significant increase in the percentage of $CD4^+$ (p=0,0079) among total tumour cells in the group treated with the SFV/IFNg compared to the PBS group, while percent of T-lymphocytes ($CD3^+$) did not differ (Fig. 8a, b). Remarkably, CD8-positive cells increased in both groups treated with SFV vectors compared to the PBS group (p=0,0476 for both) (Fig. 8c). Furthermore, the decrease in the T-reg population ($CD25^+/FoxP3^+/CD4^+$) was characteristic of the group treated with IFNg compared to the SFV/Luc group (p<0,0040) and the PBS group (p<0,0278; Fig. 8). These results clearly demonstrated that tumour treatment with the SFV vector led to an increase in the Th and CTL cell populations within the tumour, furthermore, the intra-tumoural expression of IFNg downregulates the representation of tumour-promoting T-regs in the $CD4^+$ population.

The analysis of myeloid cell populations *in vivo* is not a trivial task because these cells are highly heterogeneous and express overlapping markers at various stages of maturation. Basic phenotypic classification of myeloid cells is based on the CD11b surface marker, which is highly expressed on myeloid cells, including tumour associated macrophages (TAMs). We observed a significant decrease in $CD11b^+$ cells in the SFV/IFNg-treated tumours compared to those in the PBS group (p=0,004) (Fig. 9a). The SFV/Luc group revealed a high variability of $CD11b^+$ cells. Still, there was a positive correlation of

Preprints (www.preprints.org) | NOT PEER-REVIEWED | Posted: 30 August 2021 doi:10.20944/preprints202108.0536.v1

CD11b % and tumour weight (Pearson's correlation coefficient r=0.9249; p=0.0244), indicating that small tumours are characterized by low number of CD11b expressing myeloid cells (Supplementary Fig. S5a). Similar results were obtained in the M1 co-injected tumours (Fig. 5a). Interestingly, the CD11b^{high} population within CD11b^{+} cells was decreased both in the groups treated with SFV/IFNg and with SFV/Luc compared to the PBS group (although the latter with a lower significance, (p=0,0278 and p=0,0476, respectively) (Fig. 9a). We also observed a decrease in protumorigenic CD11b^{+}/CD206^{+} M2 macrophages in the SFV-treated tumours compared to the PBS-treated tumours (p=0,0040 for both SFV/IFNg and SFV/Luc; Fig. 9a). The CD11b^{+}/CD206^{+} cells were highly positive for Arginase 1, confirming their M2 phenotype (Supplementary Fig. S6a). Percentage of CD206^{+} cells in CD11b cell population did not change (Supplementary Fig. S6b).

CD11b^{+}/MHCII^{high} cells are considered to be antigen-presenting cells. We did not observe any significant difference in the MHCII^{high} cell population among either the total, or the CD11b^{+} cell populations (Fig. 9b). At the same time, we observed a significant decrease in the CD11b-positive/MHCII-negative population in the tumours treated with SFV/IFNg compared to that of the PBS group (p=0.0476; Fig. 9b), which indirectly indicated a decrease in the population of undifferentiated myeloid cells.

In terms of analysis of cell size and granularity of myeloid cells, we did not observe differences in the SSC-A/FSC-A populations (P1, P3, P4, Fig. 7) between groups of mice, except that in the virus-treated tumours, a significant predominance of MHCII^{+} cells in the P3 population was revealed (not shown). Nevertheless, in total tumour cells, the MHCII marker did not change between groups and populations. Interestingly, MHCII was predominantly found in the P4 population (up to 90% of CD11b^{+} cells were MHCII positive in P4), CD206^{+} cells andArginase1^{high} cells were concentrated in the P1 population, and Arginase1^{high} cells were also found in high amounts in P4, therefore forming two distinct populations (P1 and P4), which correlated with the distribution of CD11b^{+} cells (predominantly found in P1 and P4) (not shown). The CD38 and iNOs markers were widely distributed among the SSC-A/FSC-A populations. As expected, the P2 population did not contain CD11b^{+} cells or MHCII^{+} cells.

CD38 is a marker recently proposed for immunophenotyping of M1 macrophages [53,54]. This finding is highly specific for in vitro studies of BMDM polarization to M1, as we also confirmed in this study (Fig. 2). However, in tumours for in vivo TME characterization, the literature largely indicates an immunosuppressive role of the CD38 marker [55-57], which is shown to be associated with myeloid-derived suppressor cells (MDSCs) and T-regs. In that context, we do not consider tumour CD11b^{+}/CD38^{+} cells as M1 macrophages. While the impact of CD38 on macrophage phenotyping in vivo remains to be elucidated, we still included CD38 marker in our antibody panel to characterize modulation of its intra-tumoural expression by SFV vector treatment. We observed a decrease in CD11b^{+}/CD38^{+} cells in the tumours treated with the SFV vector (Fig. 9c). Moreover, the expression of IFNg led to a more significant decrease in the CD11b^{+}/CD38^{+} population (SFV/IFNg compared to the PBS group p= 0,0040; SFV/Luc compared to the PBS group p=0,0198). We observed a decrease in the expression of CD38 marker in both CD11b^{+} and CD11b^{-} populations of SFV/IFNg treated tumors compared to PBS tumors (Fig. 9c). Since CD38 is known to be also expressed on non-myeloid cells, including T-regs [58], a decrease in the CD11b^{-}/CD38^{+} population in SFV treated tumors could be associated with a decrease in the populations of T-regs (Fig. 8a).

Finally, we analysed the expression levels of Arginase 1 and iNOs in the CD11b^{+} population as immunosuppressive (Arginase 1) or inflammatory (iNOs) markers, respectively. In general, we did not find differences in the total expression levels of these enzymes between the groups. However, surprisingly, Arginase 1^{+}/iNOs^{-} cells increased in the CD11b^{+} population in the tumours treated with SFV/IFNg (PBS compared to SFV/IFNg p=0,0278; SFV/Luc compared to SFV/IFNg p=0,0476) (Fig.9d). Furthermore, iNOs^{+}/Arginase 1^{-} cells increased in the CD11b^{+} population of tumours treated with SFV/IFNg (PBS compared to SFV/IFNg p= 0,0476). Although there were no differences in the iNOs^{+}/Arginase1^{-} cells between the SFV/IFNg and SFV/Luc groups, interestingly, the smallest

Preprints (www.preprints.org) | NOT PEER-REVIEWED | Posted: 30 August 2021 doi:10.20944/preprints202108.0536.v1

tumour in the SFV/Luc group demonstrated the highest number of iNOs^{+}/Arginase 1^{-} cells (Pearson's correlation coefficient r = - 0,8407; p = 0,0372) (Supplementary Fig. S5b).

In summary, we concluded that tumour treatment with SFV/IFNg led to an increase in Th and CTL cells and a decrease in T-regs in the CD4^{+} cell population. Furthermore, treatment with SFV/IFNg inhibited CD11b^{+} cell infiltration and decreased the CD206^{+} and CD38^{+} cell populations, explaining the observed inhibition of tumor growth.

Preprints (www.preprints.org) | NOT PEER-REVIEWED | Posted: 30 August 2021 doi:10.20944/preprints202108.0536.v1

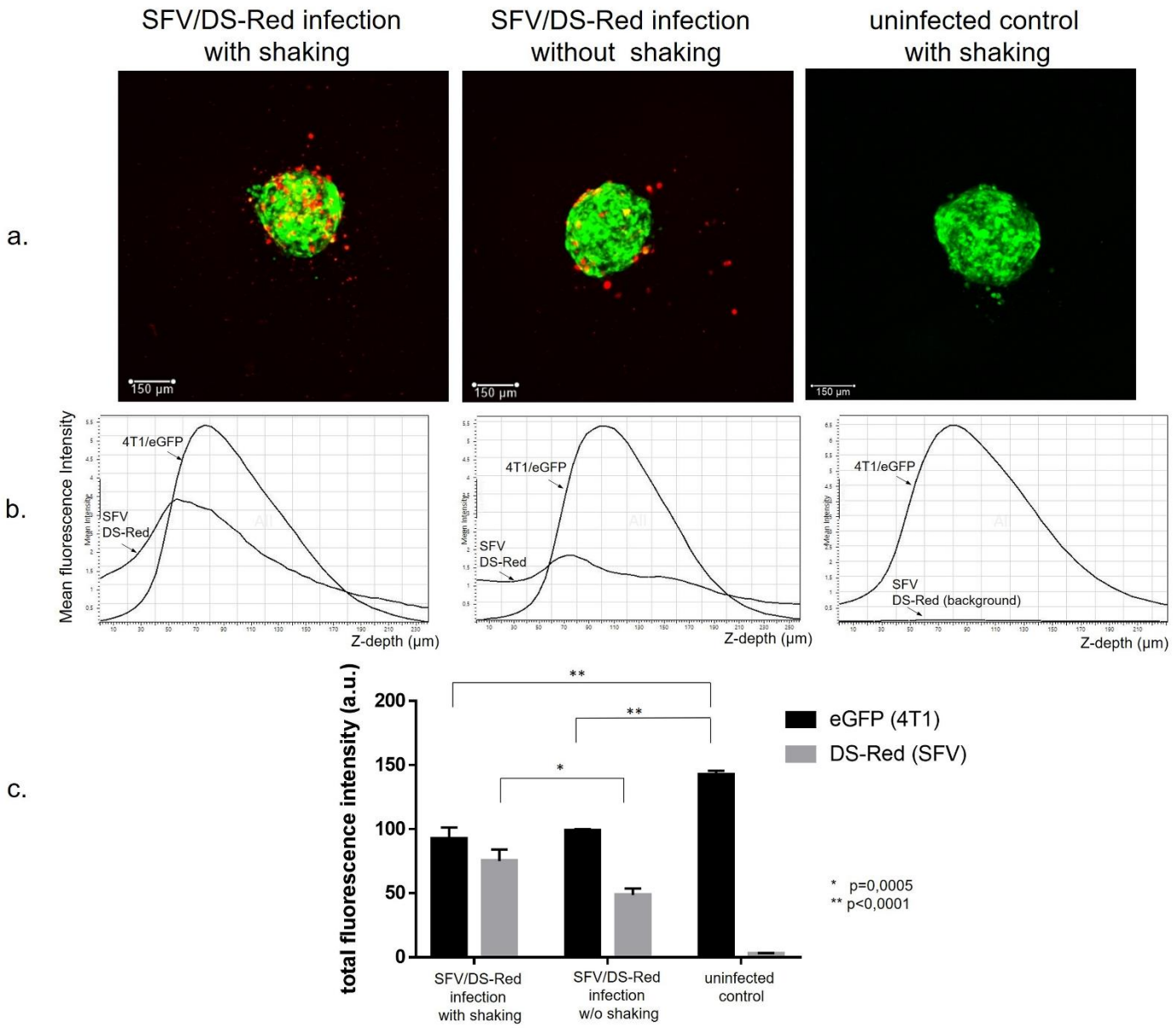

Figure 1. Infection of the 4T1/eGFP cancer cell spheroids with recombinant SFV/DS-Red virus. The 4T1/eGFP cells (3×10^3 cells per well) were plated into 96-well ultralow attachment plates. The next day, the spheroids were infected with SFV/DS-Red virus (10^5 i.u./well) either with or without shaking during incubation with the virus (1 h 10 min). Then, the spheroids were incubated for 2 days to allow DS-Red transgene expression. Confocal microscopy was performed using a Leica TCS SP8 microscope, and the images were processed by LasX software as described in the methods. **(a)** Maximum intensity projection confocal images of the 4T1/eGFP spheroids infected with SFV/DS-Red virus (representative images); **(b)** Graphical analysis of the mean fluorescence intensity changes from the spheroid upper rim to the spheroid bottom. eGFP and DS-Red signal curves are indicated by arrows; 48 planes, z step 5 µm. **(c)** Total fluorescence intensity of the spheroids incubated with or without shaking during infection and the uninfected spheroid controls**.** Data are presented as the mean of total fluorescence of four spheroids in each group. Error bars represent the standard deviation, n=4. Statistical analysis was performed by Tukey's multiple comparison test.

Preprints (www.preprints.org) | NOT PEER-REVIEWED | Posted: 30 August 2021 doi:10.20944/preprints202108.0536.v1

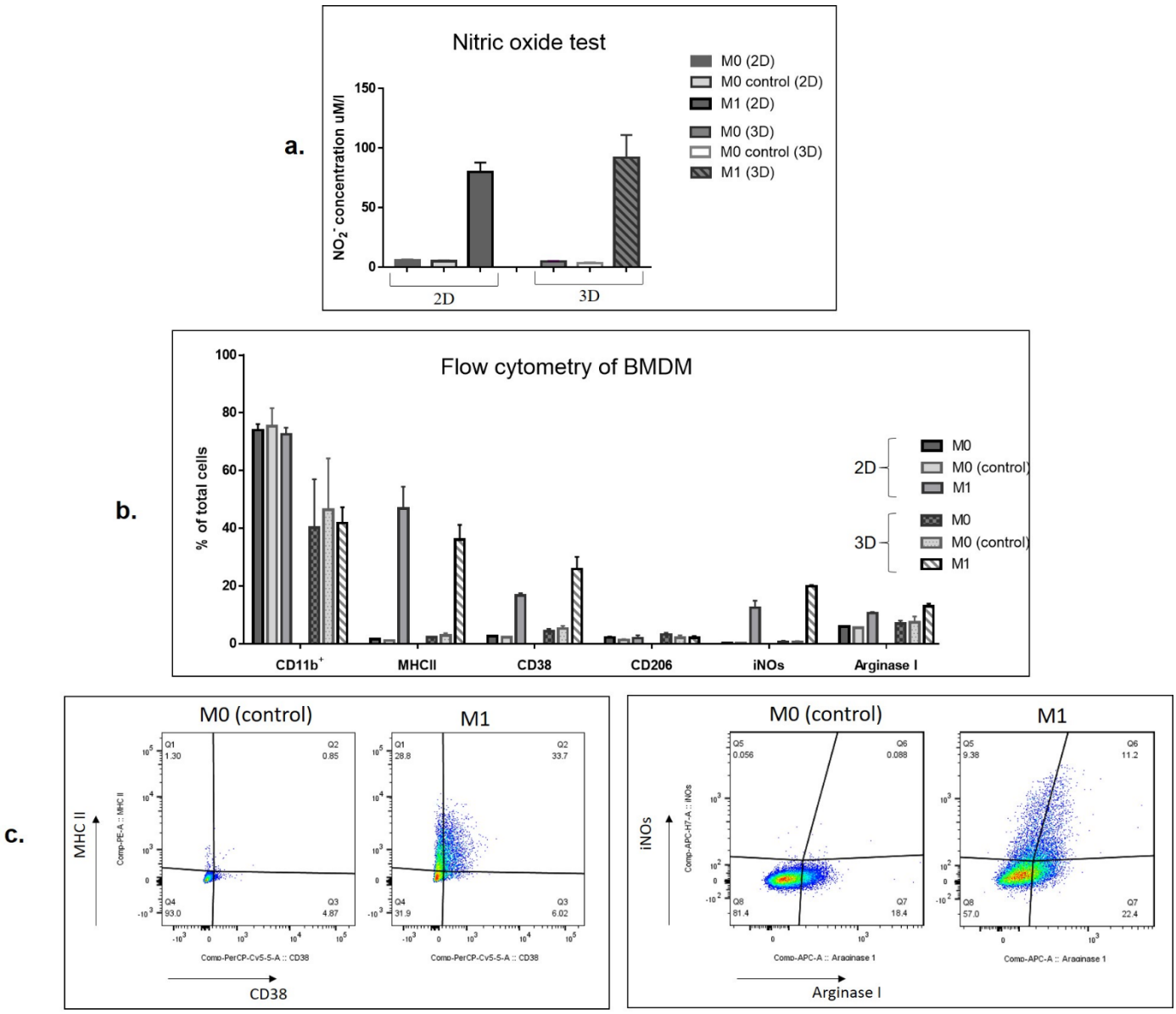

Figure 2. SFV virus-derived IFNg (vdIFNg) activates BMDMs to the M1 phenotype in monolayers (2D) and under free-floating conditions (3D). BMDMs (M0) were seeded in 12-well plates (2D) and in 96-well ultralow attachment plates and incubated for 2 days in the presence of 50 ng/ml vdIFNg and 100 ng/ml Pam3 to polarize macrophages to an M1-like phenotype (M1). M0 control represents BMDMs incubated with vdLuc supernatant (SFV/Luc conditioned medium) obtained in a similar manner as vdIFNg by infection of BHK-21 cells with the respective virus (SFV/Luc, SFV/IFNg). M0 represents untreated BMDMs. (a) Production of nitric oxide (NO) by macrophages activated to M1 under 2D and 3D conditions. The level of nitric oxide was determined in cell culture supernatants after 2 days of BMDM activation with vdIFNg under two different conditions (2D, 3D). (b) Flow cytometry analysis of macrophage surface and intracellular markers after 2 days of activation in 2D and 3D conditions. The diagram shows % of total single cells, the bars represent the mean value ± SD. (c) Representative images of flow cytometry illustrating the increase in the MHCII, CD38 and iNOs markers in M1 macrophages under 3D cultivation.

Preprints (www.preprints.org) | NOT PEER-REVIEWED | Posted: 30 August 2021 doi:10.20944/preprints202108.0536.v1

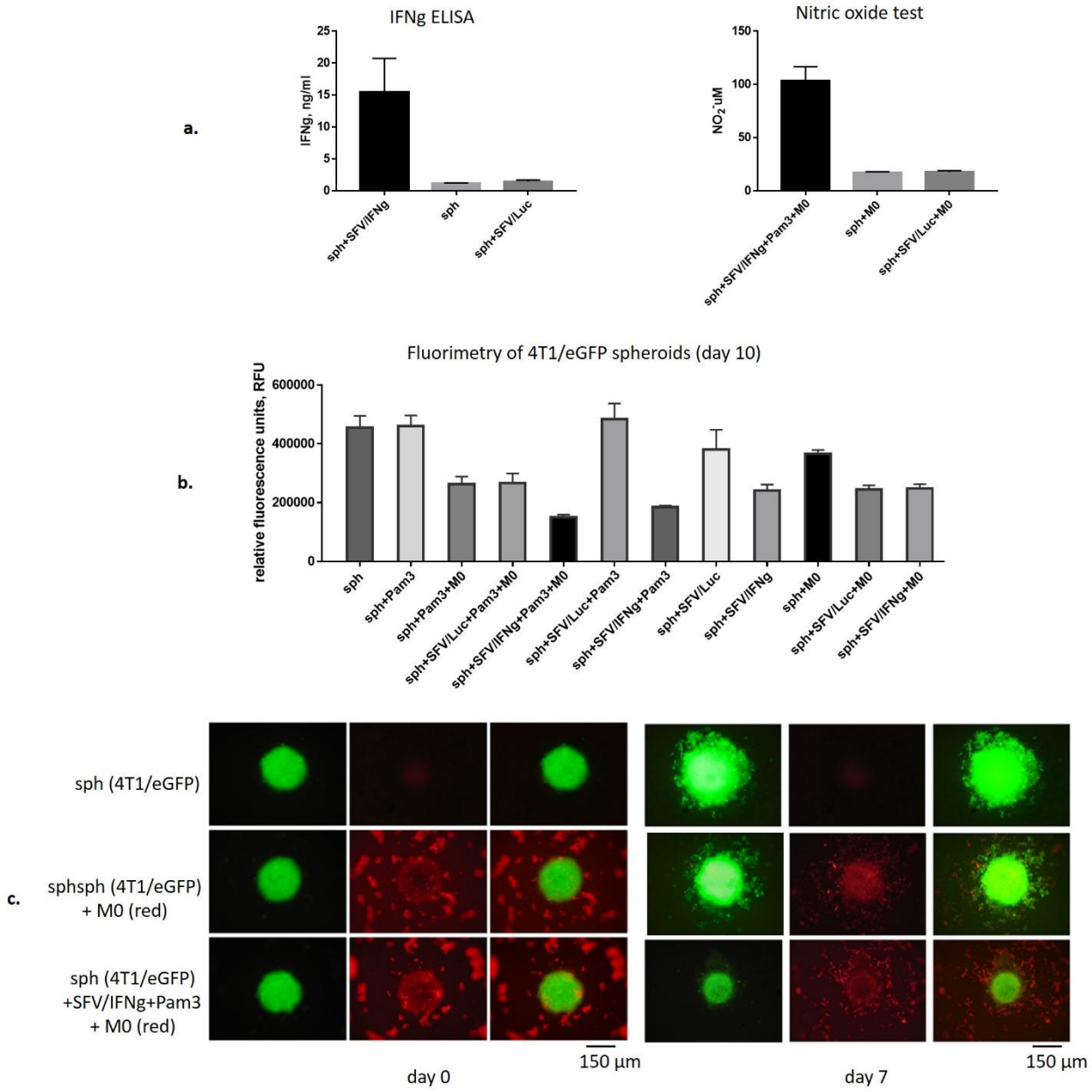

Figure 3. Coculturing of SFV/IFNg-infected 4T1/eGFP spheroids with macrophages. Single 4T1/eGFP spheroids were generated from 3000 cells in 96-well ultralow attachment plates. The next day, the spheroids were infected with either SFV/IFNg or SFV/Luc (5 ×10^4 i.u./well) or incubated with PBS as the uninfected control. The next day after infection, BMDMs (3 × 10^4 cells/well) were added to the spheroids (+M0, day 0). In total, twelve combination groups (six single spheroids in each group, n=6) were prepared: sph – uninfected spheroids (PBS); sph+Pam3; sph+Pam3+M0; sph+SFV/Luc+Pam3+M0; sph+SFV/IFNg+Pam3+M0; sph+SFV/Luc+Pam3; sph+SFV/IFNg+Pam3; sph+SFV/Luc; sph+SFV/IFNg; sph+M0; sph+SFV/Luc+M0; sph+SFV/IFNg+M0. Pam3 was added to a final concentration 100ng/ml to respective groups. **(a)** The production of vdIFNg by spheroids was measured in cell culture supernatants by ELISAs 18h after infection, before the macrophages were added. The production of NO by macrophages was measured in cell culture supernatants after two days of incubation with infected spheroids. **(b)** The total eGFP fluorescence measured by fluorimetry at day 10 of the incubation. **(c)** Representative fluorescence microscopy images of spheroids incubated with prestained macrophages (red) at day 0 and day 7. Bars represent the mean value ± SD, n=6.

Preprints (www.preprints.org) | NOT PEER-REVIEWED | Posted: 30 August 2021 doi:10.20944/preprints202108.0536.v1

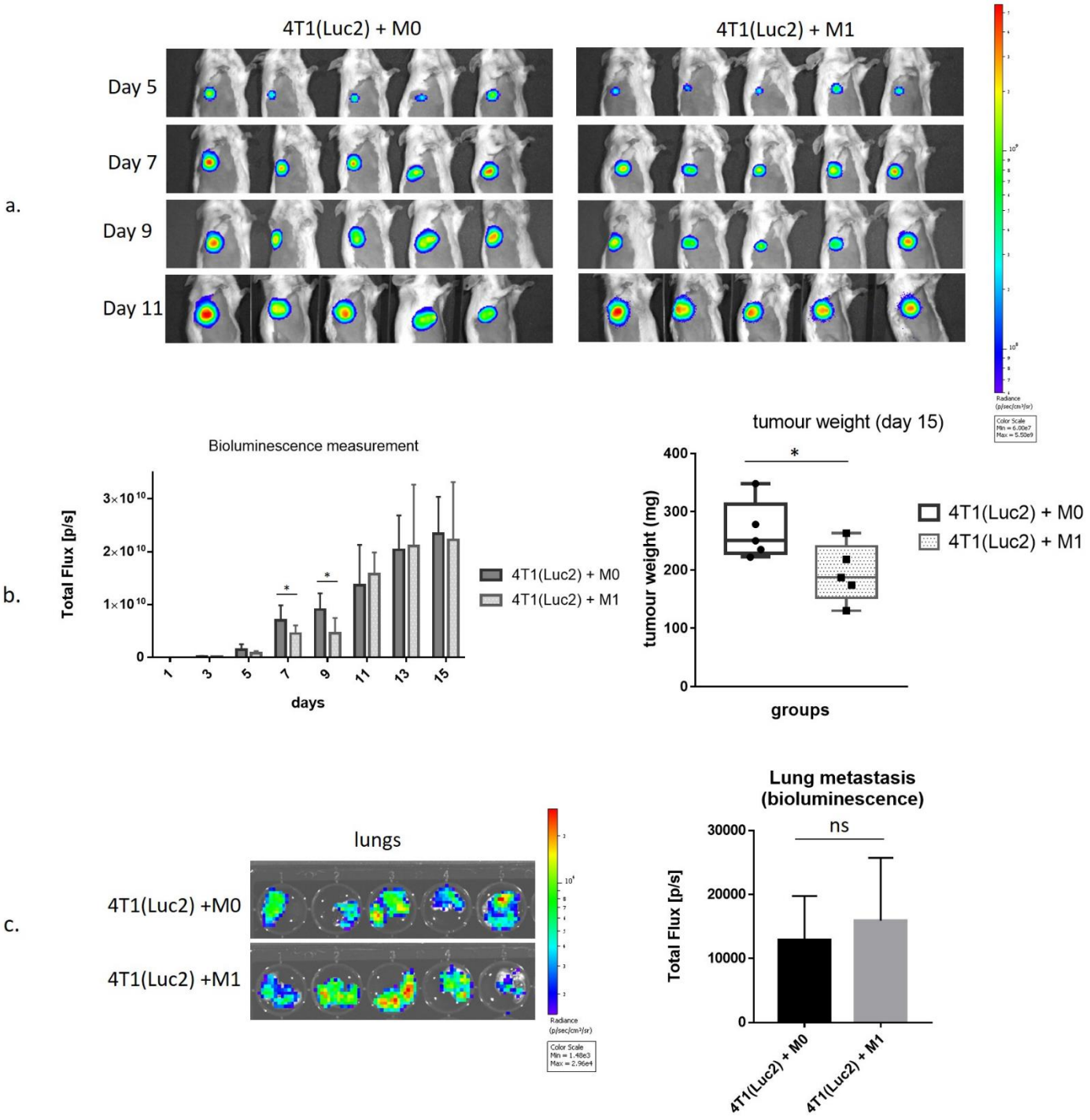

Figure 4. The effect of M1 macrophages polarized by SFV-derived IFNg on 4T1(Luc2) tumour growth. The 4T1(Luc2) cells (1×10^4) were orthotopically coinjected with 2×10^4 M0 (4T1(Luc2)+M0) or M1 (4T1(Luc2)+M1) macrophages in BALB/c mice (n=5 per group), day 0. **(a)** *In vivo* bioluminescent imaging of 4T1(Luc2) tumours expressing luciferase (days 5-11). **(b)** Quantitative analysis of tumour bioluminescence and the tumour weights. **(c)** Bioluminescence imaging of lungs isolated from the tumour-bearing mice. Bars represent the mean ± SD (n = 5); * - significant difference ($p<0.05$); ns – non-significant.

Preprints (www.preprints.org) | NOT PEER-REVIEWED | Posted: 30 August 2021 doi:10.20944/preprints202108.0536.v1

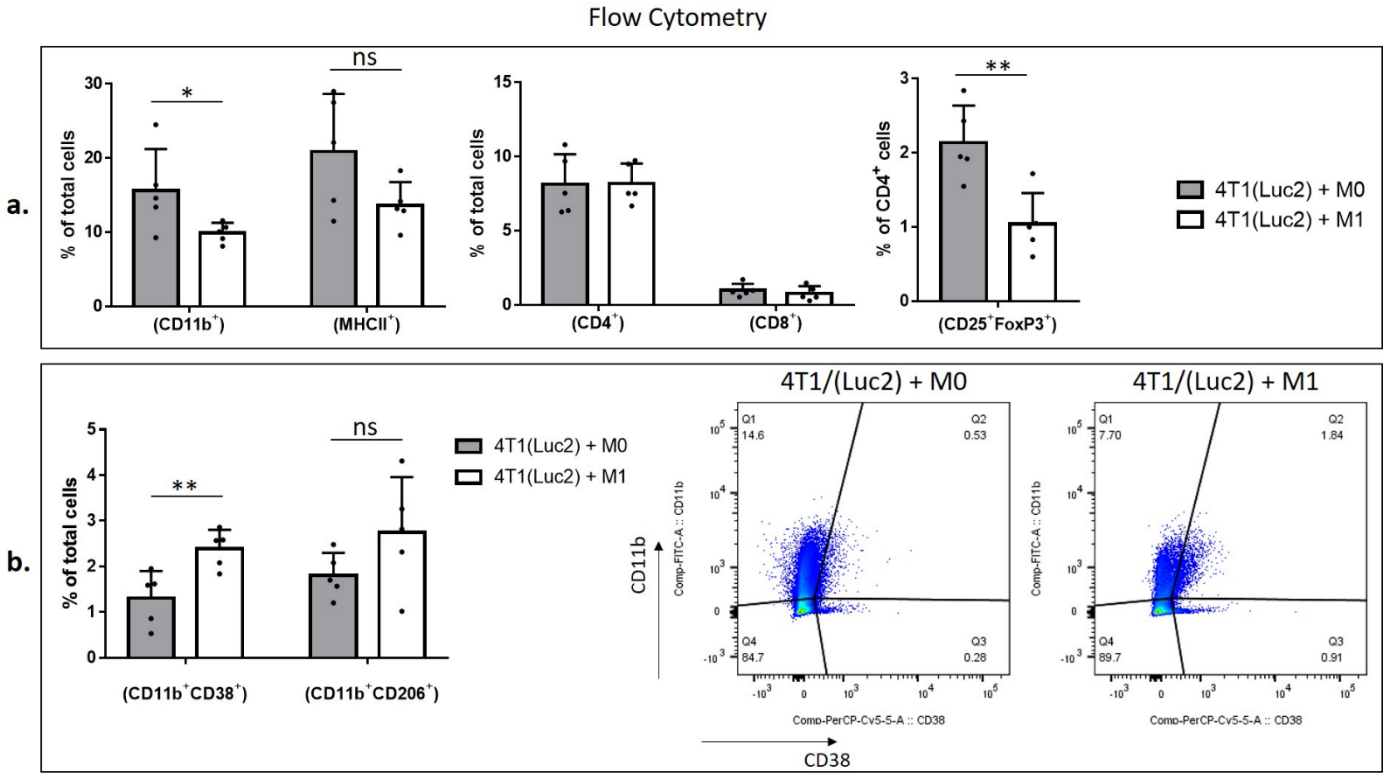

Figure 5. Flow cytometry analysis of immune cells isolated from tumours generated by implantation of 4T1(Luc2) cells premixed with M0 or M1 macrophages. Tumours were homogenized and a single cell suspension was used for immunostaining (see Materials and methods for the details). Flow cytometry was performed to quantify the immune cell populations (%): (a) $CD11b^+$; $MHCII^+$; $CD4^+$; $CD8^+$ in total single cells and $CD25^+/FoxP3^+$ in the $CD4^+$ population; and (b) double positive $CD11b^+/CD38^+$, $CD11b^+/CD206^+$ cells in total single cells. Representative flow cytometry gating data of $CD11b^+$ and $CD38^+$ cells are shown. Bars represent the mean ± SD (n = 5); * $p<0.05$; ** $p<0.01$; ns – nonsignificant.

Preprints (www.preprints.org) | NOT PEER-REVIEWED | Posted: 30 August 2021 doi:10.20944/preprints202108.0536.v1

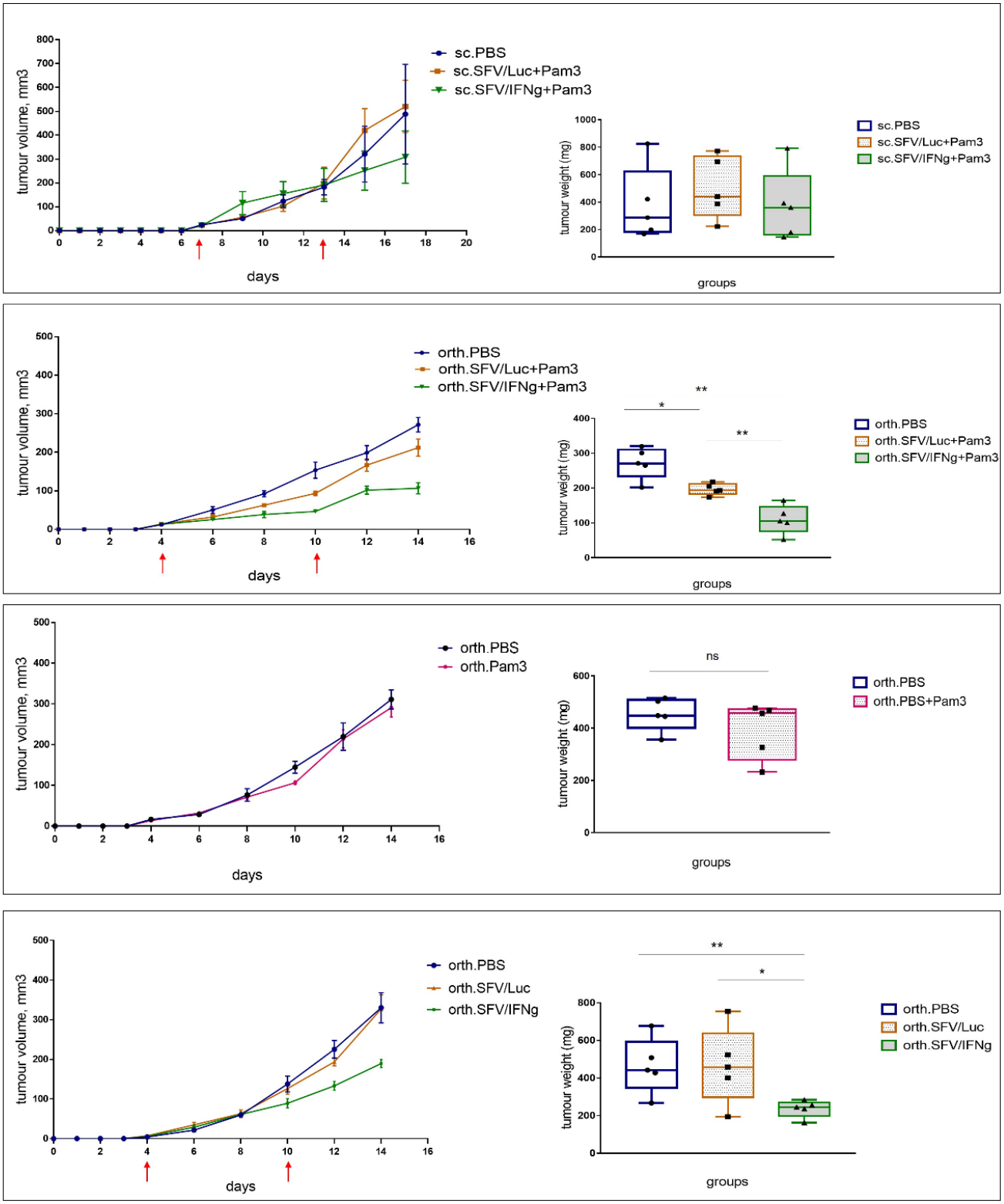

Figure 6. Inhibition of 4T1 tumour growth by i.t. injection of SFV/IFNg virus. The 4T1 mouse breast tumours were established by subcutaneous (sc.), or orthotopic injections of 2.5×10^5 and 1.25×10^5 4T1 cells, respectively. Mice received two i.t. injections of SFV vectors (4×10^7 i.u./tumour) or PBS control, as indicated by red arrow time points. The tumour growth curves are shown on the left, and the tumour weights of the groups are shown on the right. **(a)** Treatment of subcutaneous tumours with SFV/IFNg, SFV/Luc and PBS (control). The next day after virus administration, mice in these groups received i.t. injections of Pam3 solution (10 μg/tumour at day 8 after first virus administration and 15 μg/tumour at day 14 after second virus administration). **(b)** Treatment of orthotopic tumours with SFV/IFNg, SFV/Luc and PBS (control). The day after virus administration, mice in these groups received, similarly, i.t. injections of Pam3 solution (10 μg/tumour at day 5 after first virus administration and 15 μg/tumour at day 11 after second virus

Preprints (www.preprints.org) | NOT PEER-REVIEWED | Posted: 30 August 2021 doi:10.20944/preprints202108.0536.v1

administration). **(c)** Treatment of orthotopic tumours only with Pam3 (or PBS) solution: first Pam3 (10 µg/tumour) i.t. injection at day 5; second Pam3 i.t. injection (15 µg/tumour) at day 11. **(d)** Treatment of orthotopic tumours only with SFV/IFNg, SFV/Luc and PBS (control), without the subsequent Pam3 injection. Bars represent the mean ± SD (n = 5); * p<0.05; ** p<0.01; ns – nonsignificant.

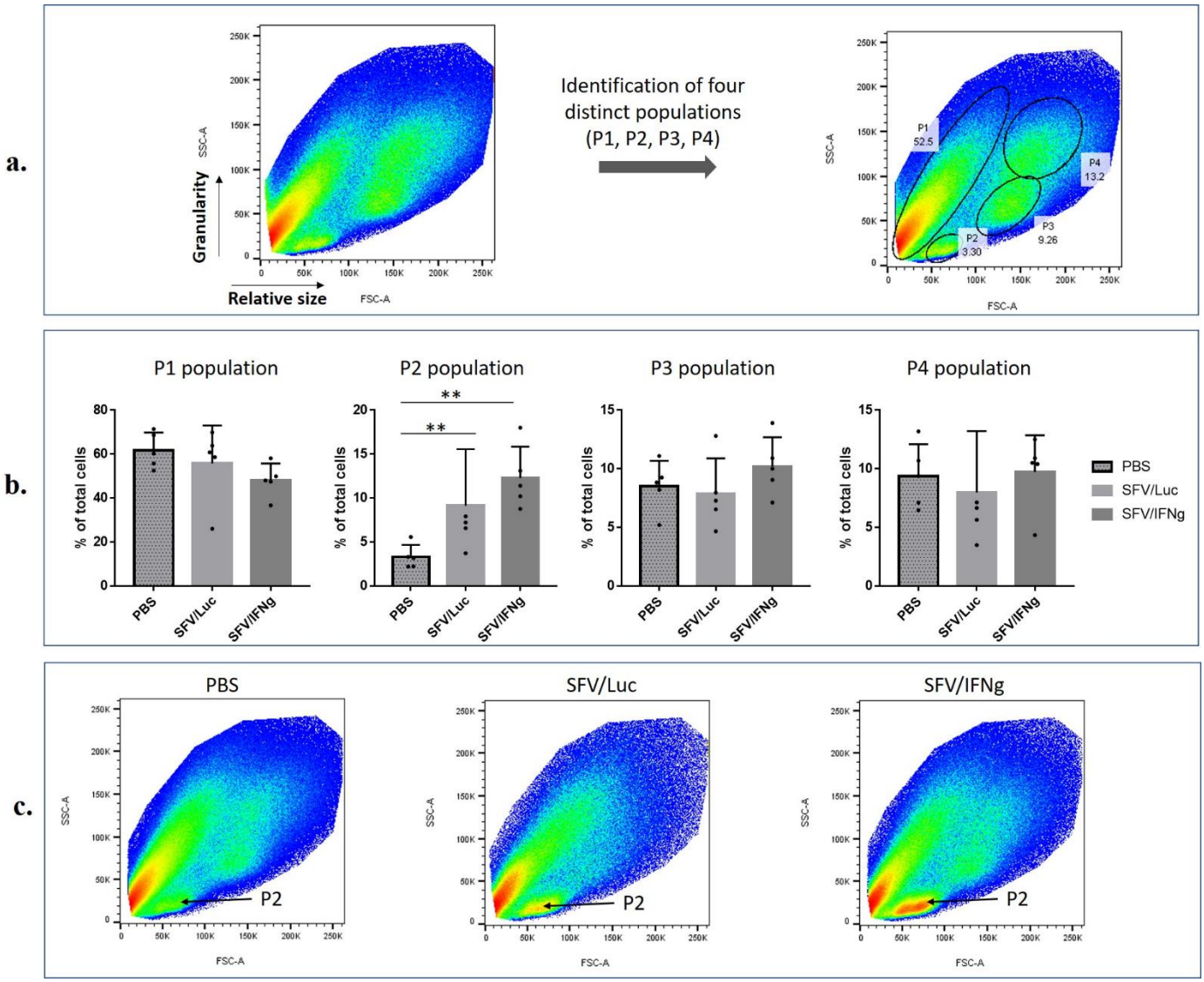

Figure 7. Flow cytometry of the 4T1 tumours treated with SFV/IFNg, SFV/Luc or PBS (mice were treated as presented in Figure 6d). Tumours were resected, homogenised to obtain a single single cell suspension, and the total isolated cells were subjected for immunostaning followed by analysis of forward and side (SSC-A/FSC-A) scattering of cell populations. **(a)** Schematic representation of the identification of four distinct single-cell populations (representative pictures). **(b)** Percentage of the respective population within total single cells (five mice per group). **(c)** Representative SSC-A/FSC-A data from the PBS, SFV/Luc, and SFV/IFNg groups. The pronounced P2 populations are indicated by arrows. Bars represent the mean ± SD (n = 5); ** p<0.01.

Preprints (www.preprints.org) | NOT PEER-REVIEWED | Posted: 30 August 2021 doi:10.20944/preprints202108.0536.v1

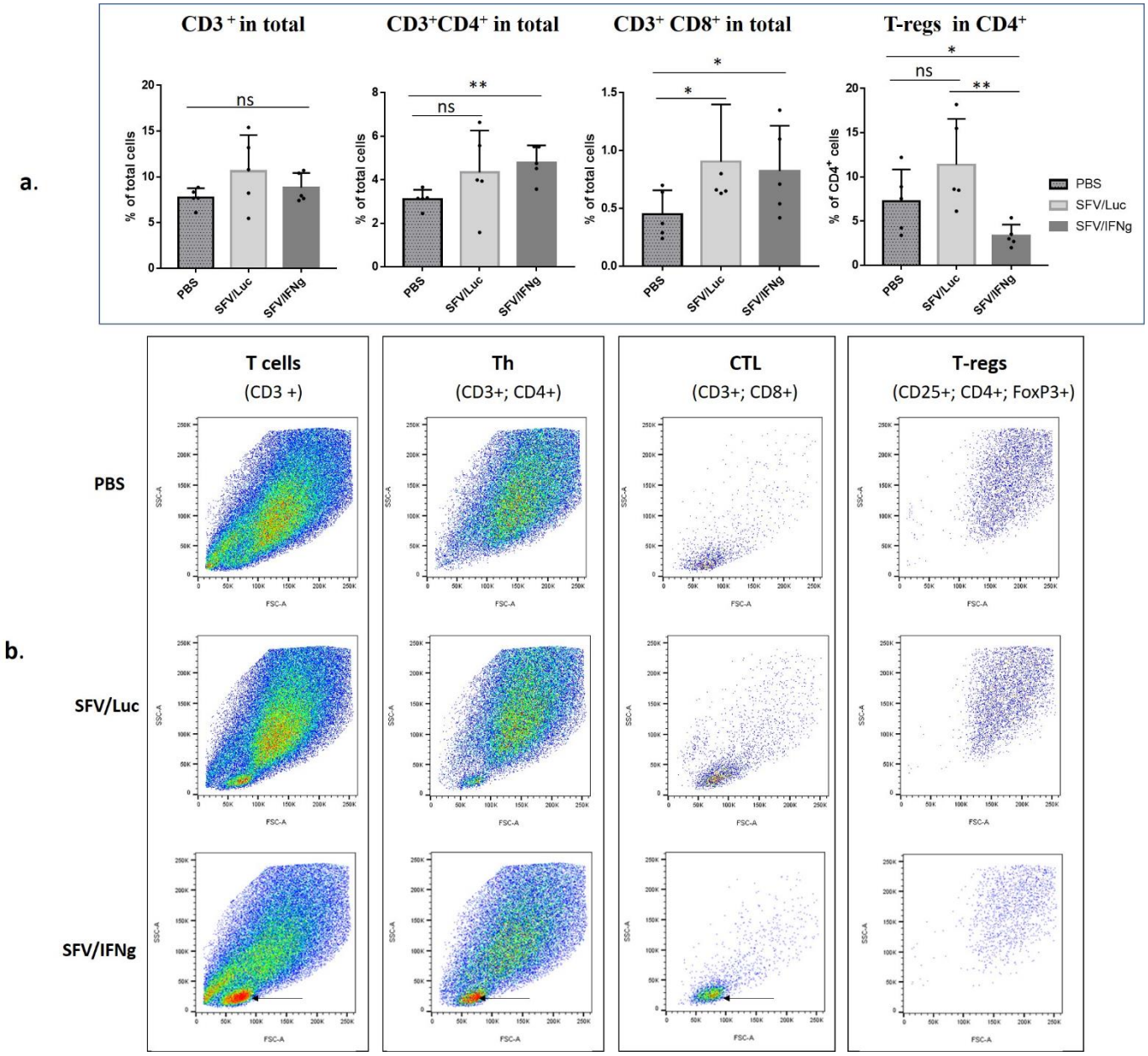

Figure 8. Flow cytometry analysis of T cells in the tumours treated with SFV/IFNg, SFV/Luc or PBS in orthotopic 4T1 mouse breast cancer model (mice were treated as presented in Figure 6d). Resected tumours were homogenized to obtain a single cell suspension, which was used for immunostaining with antibodies against surface markers (CD3, CD4, CD8, CD25) and intracellular markers (FoxP3) in one mixture. (a) Percentage of cell populations: Th cells were identified as $CD3^+/CD4^+$; CTL cells as $CD3^+/CD8^+$; T-regs as $CD4^+/CD25^+/FoxP3^+$ populations. (b) Representative pictures of forward and side (SSC-A/FSC-A) scattering of the cell populations. Arrows indicate the increased population of lymphocytes in the SFV/IFNg group. Bars represent the mean ± SD (n = 5); * $p<0.05$; ** $p<0.01$; ns – nonsignificant.

Preprints (www.preprints.org) | NOT PEER-REVIEWED | Posted: 30 August 2021 doi:10.20944/preprints202108.0536.v1

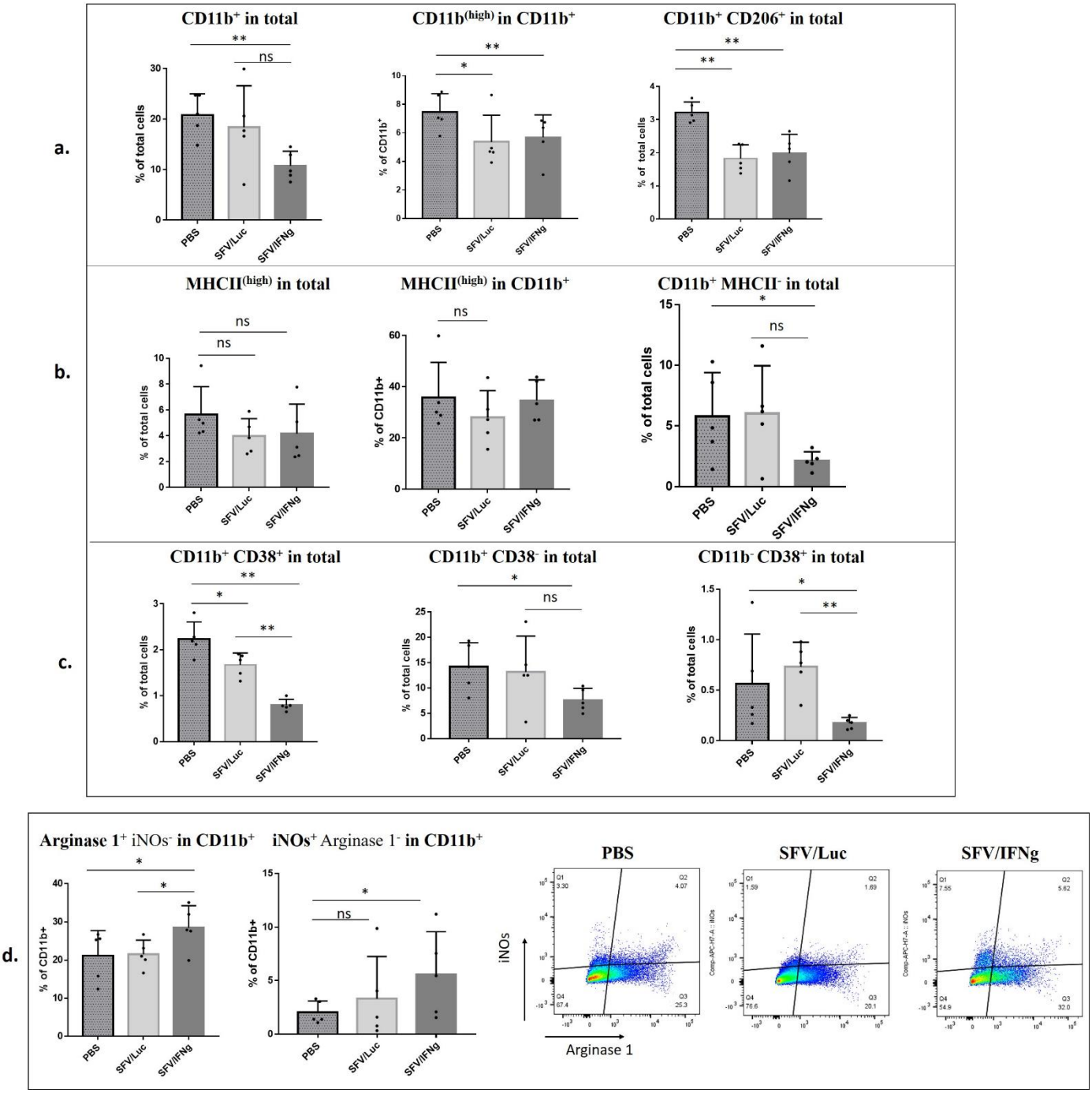

Figure 9. Flow cytometry analysis of myeloid cells in the tumours treated with SFV/IFNg, SFV/Luc or PBS in an orthotopic 4T1 mouse breast cancer model. Mice were treated as presented in Figure 6d. Resected tumours were homogenized to obtain a single cell suspension, which was used for immunostaining with antibodies against surface markers (CD11b, CD206, MHCII, CD38) and intracellular markers (Arginase 1, iNOs) in one mixture. (a) Percentage of surface markers CD11b, CD11b(high), and double positive CD206/CD11b. (b) Percentage of surface markers intracellular markers (Arginase 1; iNOs, inducible NO synthase); representative images of Arginase 1 and iNOs gating in the CD11b+ population are shown. Bars represent the mean ± SD (n = 5); * $p<0.05$; ** $p<0.01$; ns – nonsignificant.

Preprints (www.preprints.org) | NOT PEER-REVIEWED | Posted: 30 August 2021 doi:10.20944/preprints202108.0536.v1

4. Discussion

In this study we have evaluated the therapeutic potential of SFV/IFNg vector in three-dimensional (3D) *in vitro* system and in the mouse breast cancer model *in vivo*. Currently, there is no reliable 3D model to investigate the interplay between cancer cells, immune cells and viral vectors *in vitro*. We have designed and for the first time tested the cancer cell spheroid-based model for SFV vector delivery of IFNg, and its ability to activate macrophages under free floating conditions.

Similar to many other cancer cells, 4T1 cells can form spheroids in nonadherent conditions [59]. As shown in several studies, 3D cultivation results in physiologically and (epi)genetically relevant features of solid tumours, including different zones of proliferation, an oxygen gradient, a natural extracellular environment, an increased stemness-related gene expression pattern and stimulation of epithelial to mesenchymal transition-related gene expression [60-63]. Previously, numerous attempts were made to establish 4T1-based 3D/spheroid tumor model. The first one employed coculture of 4T1 cells with murine embryonic fibroblasts on matrigel [64]. Tumor-surrounding fibroblasts played a role in the distributing and connecting epithelial breast cancer cells to mimic tumour microenvironment [64]. In this, and in settings using alginate matrix, coculturing with fibroblasts (especially, NIH/3T3 cells) significantly supported the proliferation, scattering, and invasiveness of 4T1 cells [64,65]. There are also other systems for culturing cells in spheroids, using other hydrogels, diverse scaffolds or hanging drops method [66]. Here, we for the first time established a reproducible and relatively simple 3D spheroid model based solely on 4T1 cultured without a scaffold or hydrogel support, to further use it to study the susceptibility of 3D cultured tumour cells to immunotherapy with activated macrophages and viral vectors.

The main problems of viral-based therapy are low efficacy of vector delivery and poor distribution within the tumour. Indeed, while oncolytic viruses are highly efficient in killing tumour cells in vitro in a 2D monolayer, their efficiency is significantly lower in a 3D environment, both in vitro and in vivo. Due to this, prior to in vivo application, the virotherapy has to be pre-tested in the 3D tumor cell-culture systems [67]. Spatial dimension in the spheroid allows to mimic the dynamics of virus spread in the tumor and through this, optimize the treatment [67,68]. Here, we for the first time applied a spheroid-based cancer model to characterize anti-tumoural activity of virotherapy with Semliki Forest Virus vectors made to encode IFNg (SFV/IFNg). In general, the spheroid system established here allows real-time monitoring of spheroid infection and virus distribution as a small 3D tumour model. Infection of the 4T1 spheroids with SFV/DS-Red virus clearly shows the limited distribution of virus within the spheroid (Fig. 1), which, in general, reflects the *in vivo* conditions.

The addition of immune cells to the 3D system is a prerequisite for *in vitro* TME modelling. We added BMDMs to the infected spheroids to evaluate the effect of virus-derived IFNg (vdIFNg) on spheroid growth. As shown in Fig. 2, vdIFNg in the presence of TLR2/1 ligand Pam3 efficiently activated macrophages to the M1 phenotype in 3D plates, demonstrating a marker profile similar to that of monolayer conditions. We expected that nitric oxide (NO) produced by activated macrophages would inhibit the growth of 4T1/eGFP spheroids; furthermore, IFNg was shown to have a direct antiproliferative effect on cancer cells [69,70], providing strong evidence of spheroid inhibition in the presence of M1 and vdIFNg. As expected, the highest inhibitory effect was observed in the spheroids infected with SFV/IFNg in the presence of M0 macrophages and Pam3 at day 10 (Fig. 3b). Surprisingly, SFV/Luc infection also inhibited spheroid growth in the presence of M0 macrophages. This indicated possible sensitization/polarization of macrophages by SFV/Luc + Pam3 (without IFNg). Importantly, Pam 3 on its own did not affect macrophage polarization or 4T1 cell growth under 2D and 3D conditions. Nevertheless, sensing of macrophages by SFV/Luc + Pam3 without vdIFNg or in the presence of recombinant “pure”

Preprints (www.preprints.org) | NOT PEER-REVIEWED | Posted: 30 August 2021 doi:10.20944/preprints202108.0536.v1

IFNg (nonviral) may have potential for analysis of possible synergy of the antiviral immune response and M1 polarization, which is the subject of further studies.

Cell infection with alphaviruses induces a type I IFN response and results in the expression of other cytokines and chemokines by infected cells [71,72]. Macrophages express receptors for all three types of IFNs, which stimulate the expression of hundreds of genes that are known as IFN-stimulated genes (ISGs). Although BMDMs are not activated in vitro without IFNg, the presence of IFNα/β can potentially stimulate the inflammatory response in macrophages [73], which would explain the inhibitory effect of SFV/Luc+M0. This is an interesting scenario as it points that tumor virotherapy with SFV could be achieved through the induction of antiviral innate immune response leading to M1 polarization, opposing the immunosuppressive protection of virus replication at the cost of hindering the anti-tumor immune response [74].

Interestingly, we also observed inhibition of spheroid growth by M0 alone (sph+M0). Importantly, this inhibition was observed at very late days of spheroid cultivation (day 10). The total number of cells (dividing 4T1 cells and slow-dividing macrophages) or cell density, at this stage is relatively high which limits spheroid growth. Growth inhibition could be caused by limitations in the resources of the cell medium. The supply/access to oxygen, in particular, inside the spheroids, can be critical. In this respect, 3D spheroid culture may mimic the intra-tumoral hypoxia. Cycling or intermittent hypoxia occurs in solid tumors and affects different cell types in the tumor microenvironment and in particular the tumor-associated macrophages (TAMs). Interestingly, it was found to modulate the phenotype of TAMs, specifically, to polarize unpolarised (M0) murine BMDM to M1 phenotype characterized by an increase in the secretion of TNFα and IL-8/MIP-2. The pro-inflammatory phenotype of M1 macrophages induced by hypoxia was evidenced by an increased pro-inflammatory cytokine secretion and pro-inflammatory gene expression [75]. Our data indicated that this effect could be mimicked in the 3D culture at the late stages of spheroid growth, and that emerging population of M1-like cells can partially inhibit spheroid growth.

Unexpected inhibition of spheroid growth by M0 macrophages prompted us to estimate the impact of M0 and polarized M1 (vdIFNg) macrophages on tumour growth *in vivo* upon coinjection of macrophages with 4T1 (Luc2) tumour cells. Similar coinjection experiments were performed to evaluate the role of M2 macrophages prepolarized in vitro by IL-4 [76,77]. Although we observed a significant decrease in tumour weight in the 4T1(Luc2)+M1 group, tumour growth inhibition was detected only on the early days of monitoring the bioluminescence signal (Fig. 4). Furthermore, we did not observe inhibition of lung metastasis in the M1 group, indicating an insufficient therapeutic potential of M1 alone. It is widely accepted that M1 macrophages have antitumorigenic functions, whereas M2 and M0 macrophages exhibit a tumour-promoting phenotype [78]. As demonstrated in Figure 2, macrophages polarized to M1 represent a heterogeneous population because not all cells express M1 markers, and most cells probably remain M0. We can assume that these cells are partially M1 potentiated. Furthermore, high M1 plasticity was confirmed by recent studies [79,80]. Therefore, elimination of the M1 stimulus (vdIFNg) may lead to reversible reprogramming of M1 to a tumour-promoting phenotype in vivo. Nevertheless, M1 coinjection inhibited tumour weight and affected myeloid and lymphoid cell subsets by inhibiting $CD11b^+$ cell infiltration and decreasing the number of T-regs in the TME (Fig. 5), demonstrating the therapeutic potential of the M1 polarization strategy by vdIFNg.

Intratumoural administration of viral vectors expressing IFNg represents a promising strategy for immunomodulation of the TME, especially for locally advanced tumours (breast cancer, prostate cancer), which allows i.t. administration to avoid systemic toxicity of IFNg [81]. In this study, the subcutaneous model revealed high diversity of tumour growth within each group and the absence of significant inhibition of treated tumours, in contrast to the orthotopic model (Fig. 6). Subcutaneous and orthotopic models possess different biologic parameters related to tumour perfusion efficacy, hypoxic burden, microvasculature density, and immune cell infiltration, which is crucial to the

Preprints (www.preprints.org) | NOT PEER-REVIEWED | Posted: 30 August 2021 doi:10.20944/preprints202108.0536.v1

immunotherapy outcome. Orthotopic tumours usually exhibit increased malignant behaviour and less variability [82]. We revealed significant tumour inhibition specifically in an orthotopic model, which confirms the potential of the proposed SFV/IFNg vector for primary breast cancer immunotherapy.

Both treatments, the SFV/IFNg vector alone or in combination with TLR2/1 Pam3 ligand, revealed inhibition of tumour growth in the orthotopic model. Moreover, SFV/Luc in combination with Pam3 inhibited tumour growth compared to that of the PBS group. TLR agonists are known immunological adjuvants for cancer therapy and anticancer vaccines [83,84]. Pam3 was shown to reduce the suppressive function of T-regs and enhance the cytotoxicity of tumour-specific CTLs [85-87] and can inhibit tumour growth on its own [88]. Nevertheless, in our study, i.t. Pam3 injection had no effect on tumour growth (Fig. 6c). We can speculate about the synergistic effect of TLR2 agonists and SFV vectors; however, a more detailed Pam3 dose-dependent study is required to demonstrate potential synergy.

Comparison of intra-tumoral immune cell infiltrates revealed a significant increase of the T cell population in the tumours treated with SFV/IFNg. In previous studies, IFNg treatment increased the proliferation of CD4+ Th cells [89] and promoted IFNg-dependent infiltration of T-cells into tumours [90]. We observed a significant increase of the CD8 cell population in the SFV/IFNg- and SFV/Luc-treated tumours, and CD4 cells in the SFV/IFNg-treated tumours (Fig. 8). CD8 cell recruitment and activation is a characteristic feature of virus-based therapy approaches [91,92]. This dual effect of virus replication and IFNg as a CD4 effector molecule synergizes with the therapeutic outcome in treated mice. Furthermore, the decrease in the T-reg population within CD4+ cells is a complementary component of tumour growth inhibition. Low numbers of T-regs and high CD4+ and CD8+ cell:T-reg ratios are considered good prognostic factors [93,94]. IFNg can induce the fragility of tumour-derived T-regs and the loss of T-reg suppressive activity [95,96] and inhibition of T-reg expansion [97]. These data support our results of T-reg inhibition in the SFV/IFNg-treated tumours, in contrast to SFV/Luc virus treatment, which induced only an increase in the number of CD8 cells. Interestingly, M1 coinjection with cancer cells also resulted in a decrease in the T-reg cell population in CD4+ cells (Fig. 5), which can be related to IFNg-based macrophage activation and downstream related M1-T cell crosstalk through IFNg/IL-12 signaling [98].

In addition to lymphocytes, myeloid cells play an important role in TME programming. Myeloid populations such as tumour-associated macrophages (TAMs), neutrophils, and myeloid-derived suppressor cells (MDSCs) are the most abundant immune cells within tumours. We used CD11b as a typical myeloid lineage marker to characterize the infiltration of these cells in treated tumours. High $CD11b^+$ cell infiltration usually correlates with tumour progression, invasion, and metastasis [99], and patients with high $CD11b^+$ cell infiltration have a poorer surgical outcome [100]. In this study, we demonstrated a significant inhibition of the $CD11b^+$ cell population in the tumours treated with SFV/IFNg (Fig. 9a). Furthermore, the number of $CD11b^{high}$ cells was also lower in the virus-treated tumours. A similar decrease in the $CD11b^+$ population was observed in the tumours coinjected with M1 (Fig. 5a). The mechanism of the IFNg-attributed decrease in $CD11b^+$ cell infiltration is unknown. Although a linkage between the $CD11b^+$ decrease, T-reg decrease and increase in Th and CTL cells is clearly visible, the role of IFNg in immune modulation through targeting of myeloid cells remains to be unclear. It was shown previously that tumour-infiltrating T cells gradually lose their capacity to produce IFNg through post-transcriptional inhibitory events and therefore fail to clear malignant cells [101]. The exogeneous vector-based production of IFNg may directly stimulate myeloid cell differentiation to a proinflammatory phenotype to restore the IFNg/IL12 axis between M1 macrophages and T cells .

IFNg upregulates the expression of antigen presentation molecules, both MHC I and MHC II, stimulating the CTL response against cancer cells and an inflammatory Th1 adaptive response [102,103]. *In vitro* in a 3D system, we observed a significant increase of MHCII in the BMDMs treated with vdIFNg/Pam3. A relatively high level of MHCII is

Preprints (www.preprints.org) | NOT PEER-REVIEWED | Posted: 30 August 2021 doi:10.20944/preprints202108.0536.v1

classically observed on M1 macrophages. Surprisingly, we did not find any significant differences in MHCII^{high} expression on CD11b^{+} cells or CD11b^{-} cells in analyzed tumours. Nevertheless, the number of CD11b^{+}/MHC II^{-} cells decreased significantly in the SFV/IFNg-treated tumours (Fig. 9b), indicating possible differences in specific myeloid cell populations, which were not analysed in this study. More detailed analysis of MHC II levels within specific myeloid cell subsets is necessary to fully characterize the effect of SFV/IFNg treatment on MHC II levels and to unravel the mechanism vdIFNg-stimulation of lymphoid and myeloid cells in TME.

Finally, CD206 and Arginase 1 markers, which are associated with the M2-like pro-tumourigenic phenotype [47], as well as CD38 marker, which is expressed on immunosuppressive myeloid cell types [55-57], were analyzed. In this study, the decrease of CD206^{+} cells in the SFV/IFNg-treated tumours generally was assotiated with the decrease of CD11b^{+} cells infiltration (Fig.9a). Interestingly, the SFV/Luc vector also inhibited the CD206^{+} population. The virus-based inhibition of M2 can be related to the CD8-mediated response to infected cells. Remarkably, most CD206^{+} cells were highly positive for Arginase 1, confirming the M2 phenotype of these cells. Nevertheless, the analysis of the CD11b^{+} population revealed an increase in both Arginase 1 and inducible NO synthase (iNOs) in the tumours treated with SFV/IFNg (Fig. 9d), which could be attributed to the increase of expression of these markers by other cell populations (than monocytes/macrophages), such as neutrophils, indicating on complexity of the effects of SFV/IFNg vector treatment on TME, stretching beyond the macrophages [22, 104].

CD38 is expressed across different immune cell subsets, including T cells, myeloid cells, NK cells, and B cells. Recently, CD38-related immunosuppression was attributed to T-regs and MDSC populations [57,58,105]. In this study, strong inhibition of CD11b+/CD38+ (provisional MDSCs) was revealed in the tumours treated with SFV/IFNg. Interestingly, CD11b-/CD38+ (nonmyeloid cells) were also decreased in the SFV/IFNg group, indicating total CD38 marker inhibition, which can be related to the observed inhibition of T-regs, discussed above. Although the analysis of CD38 cannot directly confirm the impact of SFV/IFNg on MDSCs, the total decrease in CD38 can be considered as an important therapeutic indicator of the SFV/IFNg treatment.

The role of IFNg in the activation of myeloid-derived cells *in vivo* and *in vitro* is controversial and not completely clear. Nevertheless, the beneficial antitumour effect of SFV/IFNg shown in this study may contribute to establishing promising immunotherapies for cancer in the future. The intratumoural expression of IFNg has the potential to reprogram the TME by decreasing the populations of intra-tumoural T-regs and myeloid cells, and by activating the anti-tumour T cell subsets, enhanced by anti-proliferative qualities of IFNg in synergy with the induction of apoptosis in SFV-infected cancer cells. The application of this vector for therapeutic tuning of the TME represents a very promising strategy for the development of combined immunotherapy / chemotherapy treatments targeting different tumour escape pathways.

5. Conclusions

In this study, we showed that the SFV/IFNg vector inhibits tumour growth in an orthotopic 4T1 mouse breast cancer model. The inhibition is related to a significant increase in the population of intratumoural Th cells and CTLs, and a reduction in T-regs within Th population in tumours treated with SFV/IFNg. Furthermore, tumour growth inhibition is associated with decreased infiltration of myeloid cells expressing CD11b, CD206, and/or CD38. SFV-based expression of IFNg benefits the antitumour immune response, representing a promising adjuvant to current immunotherapy and chemotherapy strategies.

Additionally, we developed a method for coculturing cancer cell spheroids and macrophages under free-floating 3D conditions to investigate the SFV-based delivery of IFNg and to decipher the direct macrophage inhibitory effects on cancer spheroid growth. The method can facilitate various cancer research and treatment approaches, and can be useful

Preprints (www.preprints.org) | NOT PEER-REVIEWED | Posted: 30 August 2021 doi:10.20944/preprints202108.0536.v1

for modelling virus-based delivery of immune modulating genes in the presence of free-floating immune cells under 3D conditions.

Supplementary Materials. The following figures are available online: Figure S1: Analysis of 4T1/eGFP spheroids cultured in the presence of macrophages, Pam3 and SFV vectors. Figure S2: Microscopy of 4T1/eGFP spheroids cultured in the presence of macrophages, Pam3 and SFV vectors. Figure S3: Flow cytometry analysis of immune cells isolated from tumours generated by implantation of 4T1(Luc2) cells premixed with M0 or M1 macrophages. Figure S4. The tumor growth curves for all individual animals treated by i.t. injection of SFV/IFNg virus and respective controls. Figure S5. Pearson's correlation analysis of tumours treated with SFV/Luc virus in orthotopic 4T1 model. Figure S6: Flow cytometry analysis of immune cells isolated from tumours treated with SFV/IFNg, SFV/Luc viruses, or PBS in orthotopic 4T1 model.

Author Contributions: Conceptualization, A.Z; methodology, O.T., D.S., J.J., K.K., K.S.; formal analysis, O.T., A.Z., M.I.; investigation, A.Z.; resources, A.Z., M.I.; data curation, O.T., A.Z.; writing/original draft preparation, O.T., A.Z.; writing/review and editing, A.Z., M.I.; supervision, A.Z.; funding acquisition, A.Z., M.I. All authors have read and agreed to the published version of the manuscript.

Funding: This research was funded by the Latvian Council of Science, project title "Functional programming of tumor-associated macrophages with viral immunotherapy vectors in breast cancer model", project number lzp-2018/1-0208.

Institutional Review Board Statement: The study was conducted according to the guidelines of the Republic of Latvia Cabinet of Ministers No. 1 of 8 January 2019 "Regulations for the Protection of Animals Used for Scientific Purposes" and approved by the Latvian Animal Protection Ethical Committee of Food and Veterinary Service (Permit Nr. 93, from December 11., 2017, Riga, Latvia).

Informed Consent Statement:

Not applicable.

Acknowledgments: Authors would like to thank Zane Simsone, Dace Pjanova, and Felikss Rumnieks for confocal microscopy. Authors thank the Latvian Council of Science for funding of this research (project number LZP-2018/1-0208). O.T., J.J., and M.I were additionally supported by the project "New approach to active immunotherapy of hepatitis c related cancer (LIVE®VAC)", project number LZP-2018/2-0308.

Conflicts of Interest: The authors declare no conflict of interest.

References

1. Berraondo, P.; Sanmamed, M.F.; Ochoa, M.C.; Etxeberria, I.; Aznar, M. A.; Pérez-Gracia, J. L.; Rodríguez-Ruiz, M.E.; Ponz-Sarvise, M.E.; Melero, I. Cytokines in clinical cancer immunotherapy. *Br J Cancer* **2019**, *120*(1), 6-15. DOI: 10.1038/s41416-018-0328-y
2. Esquivel-Velázquez, M.; Ostoa-Saloma, P.; Palacios-Arreola, M.I.; Nava-Castro, K.E.; Castro, J.I.; Morales-Montor, J. The role of cytokines in breast cancer development and progression. *J Interferon Cytokine Res* **2015,** *35*(1), 1–16. DOI: 10.1089/jir.2014.0026
3. Castro, F.; Cardoso, A.P.; Gonçalves, R.M.; Serre, K.; Oliveira, M.J. Interferon-gamma at the crossroads of tumor immune surveillance or evasion. *Front Immunol* **2018,** *9*, 847. DOI: 10.3389/fimmu.2018.00847
4. Chin, Y.E.; Kitagawa, M; Su, W.C.; You, Z.H.; Iwamoto, Y.; Fu, X.Y. Cell growth arrest and induction of cyclin-dependent kinase inhibitor p21 WAF1/CIP1 mediated by STAT1. *Science* **1996**, *272*, 719-722. DOI: 10.1126/science.272.5262.719
5. Kalanjeri, S.; Sterman, D.H. Gene therapy in interventional pulmonology: Interferon gene delivery with focus on thoracic malignancies. *Curr Respir Care Rep* **2012**, *1*(1), 54-66. DOI: 10.1007/s13665-011-0008-3
6. Zaidi, M.R. The interferon-gamma paradox in cancer. *J Interferon Cytokine Res* **2019**, *39*(1), 30-38. DOI: 10.1089/jir.2018.0087
7. Ni, L.; Lu, J. Interferon gamma in cancer immunotherapy. *Cancer Med* **2018**, *7*(9), 4509-4516. DOI: 10.1002/cam4.1700
8. Gocher, A.M.; Workman, C.J.; Vignali, D.A.A. Interferon-γ: teammate or opponent in the tumour microenvironment? *Nat Rev Immunol* **2021**, 21 June. https://www.nature.com/articles/s41577-021-00566-3
9. Fathallah-Shaykh, H.M.; Zhao, L.J.; Kafrouni, A.I.; Smith, G.M.; Forman, J. Gene transfer of IFN-γ into established brain tumors represses growth by antiangiogenesis. *J Immunol* **2000**, *164*(1), 217-222. DOI: 10.4049/jimmunol.164.1.217.
10. Zhao, P.; Zhu, Y.H.; Wu, J.X.; Liu, R.Y.; Zhu, X.Y.; Xiao, X.; Huang, W. Adenovirus-mediated delivery of human IFNγ gene inhibits prostate cancer growth. *Life Sci* **2007,** *81*(9), 695-701. DOI: 10.1016/j.lfs.2007.05.028
11. Kanno, H.; Hattori, S.; Sato, H.; Murata, H.; Huang, F.H.; Hayashi, A.; Kaplitt, M.G. Experimental gene therapy against subcutaneously implanted glioma with a herpes simplex virus-defective vector expressing interferon-γ. *Cancer Gene Ther* **1999**, *6*(2), 147-155. DOI: 10.1038/sj.cgt.7700008

Preprints (www.preprints.org) | NOT PEER-REVIEWED | Posted: 30 August 2021 doi:10.20944/preprints202108.0536.v1

12. Zeytin, H.; Reali, E.; Zaharoff, D.A.; Rogers, C.J.; Schlom, J.; Greiner, J.W. Targeted delivery of murine IFN-γ using a recombinant fowlpox virus: NK cell recruitment to regional lymph nodes and priming of tumor-specific host immunity. *J Interferon Cytokine Res* **2008**, *28*(2), 73-87. DOI: 10.1089/jir.2007.0063
13. Dreno, B.; Urosevic-Maiwald, M.; Kim, Y.; Guitart, J.; Duvic, M.; Dereure, O.; Khammari, A.; Knol, A.C.; Derbij, A.; Lusky, M.; Didillon, I.; Santoni, A.M.; Acres, B.; Bataille, V.; Chenard, M.P.; Bleuzen, P.; Limacher, J-M.; Dummer, R. TG1042 (Adenovirus-interferon-γ) in primary cutaneous B-cell lymphomas: a phase II clinical trial. *PLoS One* **2014**. *9*(2), e83670. DOI: 10.1371/journal.pone.0083670
14. Nemunaitis, J.; Fong, T.; Burrows, F.; Bruce, J.; Peters, G.; Ognoskie, N.; Ando, D. Phase I trial of interferon gamma retroviral vector administered intratumorally with multiple courses in patients with metastatic melanoma. *Hum Gene Ther* **1999**, *10*(8), 1289-1298. DOI: 10.1038/sj.cgt.7700019
15. Schoenborn, J.R.; Wilson, C.B. Regulation of interferon-γ during innate and adaptive immune responses. *Adv Immunol* **2007**, *96*, 41-101. DOI: 10.1016/S0065-2776(07)96002-2
16. Relation, T.; Yi, T.; Guess, A. J.; La Perle, K.; Otsuru, S.; Hasgur, S.; Horwitz, E. M. Intratumoral delivery of interferonγ-secreting mesenchymal stromal cells repolarizes tumor-associated macrophages and suppresses neuroblastoma proliferation in vivo. *Stem Cells* **2018**, *36*(6), 915-924. DOI: 10.1002/stem.2801
17. Neophytou, C.M.; Pierides, C.; Christodoulou, M.I.; Costeas, P.; Kyriakou, T.C.; Papageorgis, P. The role of tumor-associated myeloid cells in modulating cancer therapy. *Front Oncol* **2020**, 10: 899. . DOI: 10.3389/fonc.2020.00899
18. Jorgovanovic, D.; Song, M.; Wang, L.; Zhang, Y. Roles of IFN-γ in tumor progression and regression: a review. *Biomark Res* **2020**, *8*(1), 49. DOI: 10.1186/s40364-020-00228-x
19. Engblom, C.; Pfirschke, C.; Pittet, M.J. The role of myeloid cells in cancer therapies. *Nat Rev Cancer* **2016**, *16*(7), 447–462. DOI: 10.1038/nrc.2016.54
20. Wu, C.; Hua, Q.; Zheng, L. Generation of Myeloid Cells in Cancer: The Spleen Matters. *Front Immunol* **2020**, *11*, 1126. DOI: 10.3389/fimmu.2020.01126
21. Ivashkiv, L.B. IFNγ: signalling, epigenetics and roles in immunity, metabolism, disease and cancer immunotherapy. *Nat Rev Immunol* **2018**, 18(9), 545–558. DOI: 10.1038/s41577-018-0029-z
22. Mojic, M.; Takeda, K.; Hayakawa, Y.; The dark side of IFN-γ: its role in promoting cancer immunoevasion. *Int J Mol Sci* **2018**, *19*(1), 89. DOI: 10.3390/ijms19010089
23. Ding, G.; Shen, T.; Yan, C.; Zhang, M.; Wu, Z.; Cao, L. IFN-γ down-regulates the PD-1 expression and assist nivolumab in PD-1-blockade effect on CD8+ T-lymphocytes in pancreatic cancer. *BMC Cancer* **2019**, *19*(1), 1053. DOI: 10.1186/s12885-019-6145-8
24. Hänze, J.; Wegner, M.; Noessner, E.; Hofmann, R.; Hegele, A. Co-regulation of immune checkpoint PD-L1 with interferon-gamma signaling is associated with a survival benefit in renal cell Cancer. *Target Oncol* **2020**, *15*, 377-390. DOI: 10.1007/s11523-020-00728-8
25. Zibelman, M. Combination of interferon-gamma and nivolumab for advanced solid tumors. ClinicalTrials.gov, Dec **2015** - Nov 2019, Identifier NCT02614456. https://clinicaltrials.gov/ct2/show/NCT02614456
26. Lv, Q.; He, C.; Quan, F.; Yu, S.; Chen, X. DOX/IL-2/IFN-γ co-loaded thermo-sensitive polypeptide hydrogel for efficient melanoma treatment. *Bioact Mater* **2018**, *3*(1), 118-128. DOI: 10.1016/j.bioactmat.2017.08.003
27. Zhou, Z.H.; Zhao, T.C.; Liang, S.Y.; Zhang, Z.Y.; Zhu, D.W.; Ju, W.T.; Zhong, L.P. (2021). A therapeutic approach with combination of interferon-gamma and autophagy inhibitor for oral squamous cell carcinoma. *Am J Cancer Res* **2021**, 11(4), 1503–1521.
28. Pyeon, D.; Vu, L,; Giacobbi, N.S.; Westrich, J.A. The antiviral immune forces awaken in the cancer wars. *PLoS Pathog* **2020**, 16(9):e1008814. DOI: 10.1371/journal.ppat.1008814
29. Brown, M.C.; Mosaheb, M.M.; Mohme, M.; McKay, Z.P.; Holl, E.K.; Kastan, J.P.; Yang, Y.; Beasley, G.M.; Hwang, E.S.; Ashley, D.M.; Bigner, D.D.; Nair, S.K.; Gromeier, M. Viral infection of cells within the tumor microenvironment mediates antitumor immunotherapy via selective TBK1-IRF3 signaling. *Nat Commun* **2021**, 12: 1858
30. Zajakina, A.; Spunde, K.; Lundstrom, K. Application of alphaviral vectors for immunomodulation in cancer therapy. *Curr Pharm Des* **2017**, *23*(32), 4906-4932. DOI: 10.2174/1381612823666170622094715
31. Singh, A.; Koutsoumpli, G.; Wall, S.; Daemen, T. An alphavirus-based therapeutic cancer vaccine: from design to clinical trial. *Cancer Immunol Immunother* **2019,** 68(5), 849-859. DOI: 10.1007/s00262-018-2276-z
32. Granot T, Meruelo D. The role of natural killer cells in combinatorial anti-cancer therapy using Sindbis viral vectors and irinotecan. *Cancer Gene Ther* **2012**, 19(8), 588–591.
33. Quetglas, J.I.; Labiano, S.; Aznar, M.A.; Bolanos, E.; Azpilikueta, A.; Rodriguez, I.; Casales, E.; Sánchez-Paulete, A.R.; Segura, V.; Smerdou, V.; Melero, I. Virotherapy with a Semliki Forest virus-ased vector encoding IL12 synergizes with PD-1/PD-L1 blockade. *Cancer Immunol Res* **2015**, 3(5), 449-54. DOI: 10.1158/2326-6066.CIR-14-0216
34. Quetglas, J.I.; Dubrot, J.; Bezunartea, J.; Sanmamed, M.F.; Hervas-Stubbs, S.; Smerdou, C.; Melero, I. Immunotherapeutic synergy between anti-CD137 mAb and intratumoral administration of a cytopathic Semliki Forest virus encoding IL-12. *Mol Ther* **2012**, 20, 1664-75.
35. Kurena, B.; Müller, E.; Christopoulos, P.F.; Johnsen, I.B.; Stankovic, B.; Øynebråten, I.; Corthay, A.; Zajakina, A. Generation and functional in vitro analysis of semliki forest virus vectors encoding TNF-α and IFN-γ. *Front Immunol* **2017**, *8*, 1667. DOI: 10.3389/fimmu.2017.01667
36. Schreiber, R.D.; Pace, J.L.; Russell, S.W.; Altman, A.; Katz, D.H. Macrophage-activating factor produced by a T cell hybridoma: physiochemical and biosynthetic resemblance to gamma-interferon. *J Immunol* **1983**, 131(2), 826-832.

Preprints (www.preprints.org) | NOT PEER-REVIEWED | Posted: 30 August 2021 doi:10.20944/preprints202108.0536.v1

37. Alexander, P.; Evans, R. Endotoxin and double stranded RNA render macrophages cytotoxic. *Nature New Biol* **1971**, 232(29), 76-78. DOI:10.1073/pnas.80.12.3782
38. Müller, E.; Christopoulos, P.F.; Halder, S.; Lunde, A.; Beraki, K.; Speth, M.; Øynebråten, I.; Corthay, A. Toll-like receptor ligands and interferon-γ synergize for induction of antitumor M1 macrophages. *Front immunol* **2017**, 8, 1383. DOI: 10.3389/fimmu.2017.01383
39. Vasilevska, J.; Skrastina, D.; Spunde, K.; Garoff, H.; Kozlovska, T.; Zajakina, A. Semliki Forest virus biodistribution in tumor-free and 4T1 mammary tumor-bearing mice: a comparison of transgene delivery by recombinant virus particles and naked RNA replicon. *Cancer Gene Ther* **2012**, *19*(8), 579-587. DOI: 10.1038/cgt.2012.37
40. Liljeström, P.; Garoff, H. A new generation of animal cell expression vectors based on the Semliki Forest virus replicon. *Biotechnol J* **1991**, *9*(12), 1356-1361. DOI: 10.1038/nbt1291-1356
41. Kurena, B.; Vežāne, A.; Skrastiņa, D.; Trofimova, O.; Zajakina, A. Magnetic nanoparticles for efficient cell transduction with Semliki Forest virus. *J Virol Methods* **2017**, *245*, 28-34. DOI: 10.1016/j.jviromet.2017.03.008
42. Hutornojs, V.; Niedre-Otomere, B.; Kozlovska, T.; Zajakina, A. Comparison of ultracentrifugation methods for concentration of recombinant alphaviruses: sucrose and iodixanol cushions. *Environ Exp Biol* **2012**, *10*, 117-123.
43. Weischenfeldt, J.; Porse, B. Bone marrow-derived macrophages (BMM): isolation and applications. *CSH Protoc* **2008,** 12, pdb-prot5080. DOI: 10.1101/pdb.prot5080
44. Davies, J.Q.; Gordon, S. Isolation and culture of murine macrophages. *Methods Mol Biol* **2005**, *290*, 91-103. DOI: 10.1385/1-59259-838-2:091
45. Baklaushev, V.P.; Kilpeläinen, A.; Petkov, S.; Abakumov, M.A.; Grinenko, N.F.; Yusubalieva, G.M.; Latanova, A.A.; Gubskiy, I.L.; Zabozlaev, F.G.; Starodubova, E.S.; Abakumova, T.O.; Isaguliants, M.G.; Chekhonin, V.P. Luciferase Expression Allows Bioluminescence Imaging But Imposes Limitations on the Orthotopic Mouse (4T1) Model of Breast Cancer. *Sci Rep* **2017** Aug 10, 7(1), 7715. DOI: 10.1038/s41598-017-07851-z.
46. Bayurova, E.; Jansons, J.; Skrastina, D.; Smirnova, O.; Mezale, D.; Kostyusheva, A.; Kostyushev, D.; Petkov, S.; Podschwadt, P.; Valuev-Elliston, V.; Sasinovich, S.; Korolev, S.; Warholm, P.; Latanova, A.; Starodubova, E.; Tukhvatulin, A.; Latyshev, O.; Selimov, R.; Metalnikov, P.; Komarov, A.; Ivanova, O.; Gorodnicheva, T.; Kochetkov, S.; Gottikh, M.; Strumfa, I.; Ivanov, A.; Gordeychuk, I.; Isaguliants, M. HIV-1 Reverse Transcriptase Promotes Tumor Growth and Metastasis Formation via ROS-Dependent Upregulation of Twist. *Oxidative Medicine and Cellular Longevity* **2019**. DOI: 10.1155/2019/6016278
47. Gordon, S. Alternative activation of macrophages. *Nat Rev Immunol* **2003**, *3*(1), 23-35. DOI: 10.1016/j.immuni.2010.05.007
48. Mantovani, A.; Allavena, P. The interaction of anticancer therapies with tumor-associated macrophages. Review J Exp Med **2015,** 212(4), 435-45. DOI: 10.1084/jem.20150295
49. El Kasmi, K.C.; Qualls, J.E.; Pesce, J.T.; Smith, A.M.; Thompson, R.W.; Henao-Tamayo, M.; Basaraba, R.J.; König, T.; Schleicher, U.; Koo, M.S.; Kaplan, G.; Fitzgerald, A.K.; Tuomanen, E.I; Orme, I.M; Kanneganti, T.D; Bogdan, C.; Wynn, T.A.; Murray, P.J. Toll-like receptor–induced arginase 1 in macrophages thwarts effective immunity against intracellular pathogens. *Nat Immunol* **2008**, 9(12), 1399-1406. DOI: 10.1038/ni.1671
50. Oldford, S.A.; Haidl, I.D.; Howatt, M.A.; Leiva, C.A.; Johnston, B.; Marshall, J.S. A critical role for mast cells and mast cell-derived IL-6 in TLR2-mediated inhibition of tumor growth. *J Immunol* **2010,** *185*(11), 7067-7076. DOI: 10.4049/jimmunol.1001137
51. Hu, H.G.; Wu, J.J.; Zhang, B.D.; Li, W.H.; Li, Y.M. Pam3CSK4-CDGSF Augments Antitumor Immunotherapy by Synergistically Activating TLR1/2 and STING. *Bioconjugate Chem* **2020,** *31*(11), 2499-2503. DOI: 10.1021/acs.bioconjchem.0c00522
52. Gorczyca, W. Atlas of Differential Diagnosis in Neoplastic Hematopathology. Published by *CRC Press*, March 21, **2014**, 919 Pages.
53. Amici, S.A.; Young, N.A.; Narvaez-Miranda, J.; Jablonski, K.A.; Arcos, J.; Rosas, L.; Papenfuss, T.L.; Torrelles, J.B.; Jarjour, W.N.; Guerau-de-Arellano, M. CD38 is robustly induced in human macrophages and monocytes in inflammatory conditions. *Front Immunol* **2018**, 9, 1593. DOI: 10.3389/fimmu.2018.01593
54. Jablonski, K.A.; Amici, S.A.; Webb, L.M.; Ruiz-Rosado, J.D.D.; Popovich, P.G.; Partida-Sanchez, S.; Guerau-de-Arellano, M. Novel markers to delineate murine M1 and M2 macrophages. *PLoS One* **2015**, 10(12), e0145342. DOI: 10.1371/journal.pone.0145342
55. Chen, L.; Diao, L.; Yang, Y.; Yi, X.; Rodriguez, B.L.; Li, Y.; Villalobos, P.A.; Cascone, T.; Liu, X, Tan, L.; Lorenzi, P.L.; Huang, A.; Zhao, Q.; Peng, D.; Fradette, J.J.; Peng, D.H.; Ungewiss, C.; Roybal, J.; Tong, P.; Oba, J.; Skoulidis, F.; Peng, W.; Carter, B.W.; Gay, C.M.; Fan, Y.; Class, C.A.; Zhu, J.; Rodriguez-Canales, J.; Kawakami, M.; Byers, L.A.; Woodman, S.E.; Papadimitrakopoulou, V.A.; Dmitrovsky, E.; Wang, J.; Ullrich, S.E.; Wistuba, I.I.; Heymach, J.V.; Qin, F.X.; Gibbons, D.L. CD38-mediated immunosuppression as a mechanism of tumor cell escape from PD-1/PD-L1 blockade. *Cancer Discov* **2018**, *8*(9), 1156-1175. DOI: 10.1158/2159-8290.CD-17-1033
56. Levy, A.; Blacher, E.; Vaknine, H.; Lund, F.E.; Stein, R.; Mayo, L. CD38 deficiency in the tumor microenvironment attenuates glioma progression and modulates features of tumor-associated microglia/macrophages. *Neuro Oncol* **2012,** *14*(8), 1037-1049. DOI: 10.1093/neuonc/nos121
57. Karakasheva, T.A.; Waldron, T.J.; Eruslanov, E.; Kim, S.B.; Lee, J.S.; O'Brien, S.; Hicks, P.D.; Basu, D.; Singhal, S.; Malavasi, F.; Rustgi, A. K. CD38-expressing myeloid-derived suppressor cells promote tumor growth in a murine model of esophageal cancer. *Cancer Res* **2015**, *75*(19), 4074-4085. DOI: 10.1158/0008-5472.CAN-14-3639
58. Patton, D.T.; Wilson, M.D.; Rowan, W.C.; Soond, D.R.; Okkenhaug, K. The PI3K p110δ regulates expression of CD38 on regulatory T cells. *PLoS One* **2011**, *6*(3), e17359. DOI: 10.1371/journal.pone.0017359

Preprints (www.preprints.org) | NOT PEER-REVIEWED | Posted: 30 August 2021 doi:10.20944/preprints202108.0536.v1

59. Upreti, M.; Jamshidi-Parsian, A.; Koonce, N.A.; Webber, J.S.; Sharma, S.K.; Asea, A.A.; Griffin, R.J. Tumor-endothelial cell three-dimensional spheroids: new aspects to enhance radiation and drug therapeutics. *Transl Oncol* **2011**, *4*(6), 365-376. DOI: 10.1593/tlo.11187
60. Melissaridou, S.; Wiechec, E.; Magan, M.; Jain, M.V.; Chung, M.K.; Farnebo, L.; Roberg, K. The effect of 2D and 3D cell cultures on treatment response, EMT profile and stem cell features in head and neck cancer. *Cancer Cell Int* **2019**, 19(1), 1-10.
61. Chaicharoenaudomrung, N.; Kunhorm, P.; Noisa, P. Three-dimensional cell culture systems as an in vitro platform for cancer and stem cell modeling. *World J Stem Cells* **2019**, 11(12), 1065.DOI: 10.4252/wjsc.v11.i12.1065
62. Gheytanchi, E.; Naseri, M.; Karimi-Busheri, F.; Atyabi, F.; Mirsharif, E.S.; Bozorgmehr, M.; Madjd, Z. Morphological and molecular characteristics of spheroid formation in HT-29 and Caco-2 colorectal cancer cell lines. *Cancer Cell Int* **2021**, 21(1), 204. DOI: 10.1186/s12935-021-01898-9
63. Kenny, P.A.; Lee, G.Y.; Myers, C.A.; Neve, R.M.; Semeiks, J.R.; Spellman, P.T.;, K.; Lee,E.H.; Barcellos-Hoff, M.H.; 1 Petersen, O.W.; 2 Gray, J.W.; Bissell, M. J. The morphologies of breast cancer cell lines in three-dimensional assays correlate with their profiles of gene expression. *Mol Oncol* **2007** 1(1), 84-96. DOI:10.1016/j.molonc.2007.02.004
64. Li, L.; Lu, Y. Optimizing a 3D culture system to study the interaction between epithelial breast cancer and its surrounding fibroblasts. *J Cancer* **2011**, 2, 458-466. DOI:10.7150/jca.2.458
65. Rama-Esendagli, D.; Esendagli, G.; Yilmaz, G.; Guc, D. Spheroid formation and invasion capacity are differentially influenced by co-cultures of fibroblast and macrophage cells in breast cancer *Mol Biol Rep* **2014**, 41(5), 2885-92. DOI: 10.1007/s11033-014-3144-3
66. Białkowska, K.; Komorowski, P.; Bryszewska, M.; Miłowska, K. Spheroids as a type of three-dimensional cell cultures-examples of methods of preparation and the most important application. *Int J Mol Sci* **2020**, 21(17), 6225. DOI: 10.3390/ijms21176225.
67. Kloker, L.D.; Yurttas, C.;Lauer, U.M. Three-dimensional tumor cell cultures employed in virotherapy research. *Oncolytic Virother* **2018**, 7: 79–93. DOI: 10.2147/OV.S165479
68. Berg, D.R.; Offord, C.P.; Kemler, I.; Ennis, M.K.; Chang, L.; Paulik, G.; Bajzer, Z.; Neuhauser, C.; Dingli, D. In vitro and in silico multidimensional modeling of oncolytic tumor virotherapy dynamics. *PLoS Comput Biol* **2019**, 15(3): e1006773. DOI: 10.1371/journal.pcbi.1006773
69. Detjen, K.M.; Farwig, K.; Welzel, M.; Wiedenmann, B.; Rosewicz, S. Interferon gamma inhibits growth of human pancreatic carcinoma cells via caspase-1 dependent induction of apoptosis. *Gut,* **2001**, 49(2), 251-62. DOI: 10.1136/gut.49.2.251.
70. Chawla-Sarkar, M.; Lindner, D.J.; Liu, Y.F.; Williams, B.R.; Sen, G.C.; Silverman, R.H.; Borden, E.C. Apoptosis and interferons: role of interferon-stimulated genes as mediators of apoptosis. *Apoptosis* **2003**, 8, 237–249. doi: 10.1023/a:1023668705040
71. Frolov, I.; Akhrymuk, M.; Akhrymuk, I.; Atasheva, S.; Frolova, E.I. Early events in alphavirus replication determine the outcome of infection. *J Virol* **2012**, *86*(9), 5055-5066. DOI: 10.1128/JVI.07223-11
72. Ryman, K.D.; Klimstra, W.B. Host responses to alphavirus infection. *Immunol Rev* **2008**, *225*(1), 27-45. DOI: 10.1111/j.1600-065X.2008.00670.x
73. Xu, Q.; Tang, Y.; Huang, G. Innate immune responses in RNA viral infection. *Front Med* **2020**, 1-14. DOI: 10.1007/s11684-020-0776-7
74. Denton, N.L.; Chen, C-Y.; Scott, T.R; Cripe, T.P. Tumor-Associated Macrophages in Oncolytic Virotherapy: Friend or Foe? B*iomedicines* **2016**, 4(3), 13. DOI: 10.3390/biomedicines4030013
75. Delprat, V.; Tellier, C.; Demazy, C.; Raes, M.; Feron, O.; Michiels, C. Cycling hypoxia promotes a pro-inflammatory phenotype in macrophages via JNK/p65 signaling pathway. *Sci Rep* **2020,** 10, 882. doi: 10.1038/s41598-020-57677-5
76. Cho, H.J.; Jung, J.I.; Kwon, G.T.; Her, S.; Park, J.H.; Park, J.H.Y. Bone marrow-derived, alternatively activated macrophages enhance solid tumor growth and lung metastasis of mammary carcinoma cells in a Balb/C mouse orthotopic model. *Breast Cancer Res* **2012,** *14*(3), R81. DOI: 10.1186/bcr3195
77. Kuwada, K.; Kagawa, S.; Yoshida, R.; Sakamoto, S.; Ito, A.; Watanabe, M.; Ieda, T; Kuroda, S.; Kikuchi, S.; Tazawa, H.; Fujiwara, T. The epithelial-to-mesenchymal transition induced by tumor-associated macrophages confers chemoresistance in peritoneally disseminated pancreatic cancer. *J Exp Clin Cancer Res* **2018**, *37*(1), 307. DOI: 10.1186/s13046-018-0981-2
78. Yuan, A.; Hsiao, Y.J.; Chen, H.Y.; Chen, H.W.; Ho, C.C.; Chen, Y.Y.; Liu, Y.C.; Hong, T.H.; Yu, S.L; Chen J.J.W.; Yang, P. C. Opposite effects of M1 and M2 macrophage subtypes on lung cancer progression. *Sci Rep* **2015**, *5*, 14273. DOI: 10.1038/srep14273
79. Wang, F.; Zhang, S.; Jeon, R.; Vuckovic, I.; Jiang, X.; Lerman, A.; Folmesb, C.D; Dzejaa, P.D.; Herrmann, J. Interferon gamma induces reversible metabolic reprogramming of M1 macrophages to sustain cell viability and pro-inflammatory activity. *EBioMedicine* **2018**, *30*, 303-316. DOI: 10.1016/j.ebiom.2018.02.009
80. Liu, S.X.; Gustafson, H.H.; Jackson, D.L.; Pun, S.H.; Trapnell, C. Trajectory analysis quantifies transcriptional plasticity during macrophage polarization. *Sci Rep* **2020**, *10*(1), 12273. DOI: 10.1038/s41598-020-68766-w
81. Sriskandan, K.; Garner, P.; Watkinson, J.; Pettingale, K.W.; Brinkley, D.; Calman, F.M.B.; Tee, D.E. A toxicity study of recombinant interferon-gamma given by intravenous infusion to patients with advanced cancer. *Cancer Chemother Pharmacol* **1986**, *18*, 63–68. DOI: 10.1007/BF00253067
82. Zhang, Y.; Zhang, G.L.; Sun, X.; Cao, K.X.; Ma, C.; Nan, N.; Yang, G.W.; Yu, M.W.; Wang, X.M. Establishment of a murine breast tumor model by subcutaneous or orthotopic implantation. *Oncol Lett* **2018**, *15*(5), 6233-6240. DOI: 10.3892/ol.2018.8113
83. Liu, C.; Han, C.; Liu, J. The Role of Toll-Like Receptors in Oncotherapy. *Oncol Res* **2019**, *27*(8), 965-978. DOI: 10.3727/096504019X15498329881440
84. Paston, S.J.; Brentville, V.A.; Symonds, P.; Durrant, L.G. Cancer Vaccines, Adjuvants, and Delivery Systems. *Fron. Immunol* **2021,** 12, 627932. DOI: 10.3389/fimmu.2021.627932

Preprints (www.preprints.org) | NOT PEER-REVIEWED | Posted: 30 August 2021 doi:10.20944/preprints202108.0536.v1

85. Zhang, Y.; Luo, F.; Cai, Y.; Liu, N.; Wang, L.; Xu, D.; Chu, Y. TLR1/TLR2 agonist induces tumor regression by reciprocal modulation of effector and regulatory T cells. *J Immunol* **2011**, *186*(4), 1963-1969. DOI: 10.4049/jimmunol.1002320
86. Amiset, L.; Fend, L.; Gatard-Scheikl, T.; Rittner, K.; Duong, V.; Rooke, R.; Muller, S.; Bonnefoy, J.Y.; Préville, X.; Haegel, H. TLR2 ligation protects effector T cells from regulatory T-cell mediated suppression and repolarizes T helper responses following MVA-based cancer immunotherapy. *Oncoimmunology* **2012**, *1*(8), 1271-1280. DOI: 10.4161/onci.21479
87. Abdel-Aal, A.B.; Lakshminarayanan, V.; Thompson, P.; Supekar, N.; Bradley, J.M.; Wolfert, M.A.; Cohen, P.A.; Gendler, S.J.; Boons, G.J. Immune and anticancer responses elicited by fully synthetic aberrantly glycosylated MUC1 tripartite vaccines modified by a TLR2 or TLR9 agonist. *Chembiochem* **2014**, *15*(10), 1508-1513. DOI: 10.1002/cbic.201402077
88. Oldford, S.A.; Haidl, I.D.; Howatt, M.A.; Leiva, C.A.; Johnston, B.; Marshall, J.S. A critical role for mast cells and mast cell-derived IL-6 in TLR2-mediated inhibition of tumor growth. *J Immunol* **2010**, *185*(11), 7067-7076. DOI: 10.4049/jimmunol.1001137
89. Reed, J.M.; Branigan, P.J.; Bamezai, A. Interferon gamma enhances clonal expansion and survival of $CD4^+$ T cells. *J Interferon Cytokine Res* **2008**, *28*, 611–622. DOI: 10.1089/jir.2007.0145
90. Reid, G.S.; Shan, X.; Coughlin, C.M.; Lassoued, W.; Pawel, B.R.; Wexler, L.H.; Thiele, C.J.; Tsokos, M.; Pinkus, J.L.; Pinkus, G.S.; Grupp, S.A.; Vonderheide RH. Interferon-gamma-dependent infiltration of human T cells into neuroblastoma tumors in vivo. *Clin Cancer Res* **2009**, *15*(21), 6602-6608. DOI: 10.1158/1078-0432.CCR-09-0829
91. Bourgeois-Daigneault, M.C.; Roy, D.G.; Falls, T.; Twumasi-Boateng, K.; St-Germain, L.E.; Marguerie, M.; Garcia, V.; Selman, M.; Jennings, V.A.; Pettigrew, J.; Amos, S.; Diallo, J.S.; Nelson, B.; Bell, J.C. Oncolytic vesicular stomatitis virus expressing interferon-γ has enhanced therapeutic activity. *Mol Ther Oncolytics* **2016**, *3*, 16001. DOI: 10.1038/mto.2016.1
92. Yamashita, M.; Tasaki, M.; Murakami, R.; Arai, Y.; Nakamura, T.; Nakao, S. Oncolytic vaccinia virus induces a novel phenotype of $CD8^+$ effector T cells characterized by high ICOS expression. *Mol Ther Oncolytics* **2021**, *20*, 422-432. DOI: 10.1016/j.omto.2021.01.016
93. Curiel, T.J.; Coukos, G.; Zou, L; Alvarez, X; Cheng, P.; Mottram P.; Evdemon-Hogan, M.; Conejo-Garcia, J.R.; Zhang, L.; Burow, M.; Zhu, Y.; Wei, S.; Kryczek, I.; Daniel, B.; Gordon, A.; Myers, L.; Lackner, A.; Disis, M.L.; Knutson, K.L.; Chen, L.; Zou, W. Specific recruitment of regulatory T cells in ovarian carcinoma fosters immune privilege and predicts reduced survival. *Nat Med* **2004**, *10*, 942-949. DOI: 10.1038/nm1093
94. Wang, J.; Tian, S.; Sun, J.; Zhang, J.; Lin, L.; Hu, C. The presence of tumour-infiltrating lymphocytes (TILs) and the ratios between different subsets serve as prognostic factors in advanced hypopharyngeal squamous cell carcinoma. *BMC Cancer* **2020**, *20*, 731. DOI: 10.1186/s12885-020-07234-0
95. Overacre-Delgoffe, A.E.; Chikina, M.; Dadey, R.E.; Yano, H.; Brunazzi, E.A.; Shayan, G.; Horne, W.; Moskovitz, J.M.; Kolls, J.K.; Sander, C.; Shuai, Y.; Normolle, D.P.; Kirkwood, J.M.; Ferris, R.L.; Delgoffe, G.M.; Bruno, T.C.; Workman, C.J.; Vignali, D.A.A. Interferon-γ drives Treg fragility to promote anti-tumor immunity. *Cell* **2017**, *169*(6), 1130–1141. DOI: 10.1016/j.cell.2017.05.005
96. Overacre-Delgoffe, A.E.; Vignali, D.A.A. Treg Fragility: A Prerequisite for Effective Antitumor Immunity? *Cancer Immunol Res* **2018**, *6*(8), 882–887. DOI: 10.1158/2326-6066.CIR-18-0066
97. Deligne, C.; Metidji, A.; Fridman, W.H.; Teillaud, J.L. Anti-CD20 therapy induces a memory Th1 response through the IFN-γ/IL-12 axis and prevents protumor regulatory T-cell expansion in mice. *Leukemia* **2015**, *29*, 947-957. DOI: 10.1038/leu.2014.275
98. Garner, H.; de Visser, K.E. Immune crosstalk in cancer progression and metastatic spread: a complex conversation. *Nat Rev Immunol* **2020**, *20*, 483–497. DOI: 10.1038/s41577-019-0271-z
99. Wu, C.; Hua, Q.; Zheng, L. Generation of Myeloid Cells in Cancer: The Spleen Matters. *Front Immunol* **2020**, *11*, 1126. DOI: 10.3389/fimmu.2020.01126
100. Okita, Y.; Tanaka, H.; Ohira, M.; Muguruma, K.; Kubo, N.; Watanabe, M.; Fukushima, W.; Hirakawa, K.; Hirakawa, K. Role of tumor-infiltrating CD11b+ antigen-presenting cells in the progression of gastric cancer. *J Surg Res* **2014**, *186*(1), 192-200. DOI: 10.1016/j.jss.2013.08.024
101. Salerno, F.; Guislain, A.; Freen-Van Heeren, J.J.; Nicolet, B.P.; Young, H.A.; Wolkersa, M.C. Critical role of post-transcriptional regulation for IFN-γ in tumor-infiltrating T cells. *Oncoimmunology* **2018**, *8*(2), e1532762. DOI: 10.1080/2162402X.2018.1532762
102. Cheon, H.; Borden, E.C.; Stark, G.R. Interferons and their stimulated genes in the tumor microenvironment. *Semin Oncol* **2014**, *41*(2), 156-173. DOI: 10.1053/j.seminoncol.2014.02.002.
103. Alspach, E.; Lussier, D.M.; Schreiber, R.D. Interferon γ and its important roles in promoting and inhibiting spontaneous and therapeutic cancer immunity. *Cold Spring Harb Perspect Biol* **2018**, *11*(3), a028480. DOI: 10.1101/cshperspect.a028480
104. Giese, M.A.; Hind,L.E.; Huttenlocher, A. Neutrophil plasticity in the tumor microenvironment. *Blood* **2019**, 133(20), 2159–2167.
105. Feng, X.; Zhang, L.; Acharya, C.; An, G.; Wen, K.; Qiu, L.; Munshi, N.; Tai, Y.T.; Anderson, K.C. Targeting CD38 suppresses induction and function of T regulatory cells to mitigate immunosuppression in multiple myeloma. *Clin Cancer Res* **2017**, *23*(15), 4290–4300. DOI: 10.1158/1078-0432.CCR-16-3192.